Local time extent of magnetopause reconnection using space-ground coordination

Ying Zou[1,2], Brian M. Walsh[3], Yukitoshi Nishimura[4,5], Vassilis Angelopoulos[6], J. Michael Ruohoniemi[7], Kathryn A. McWilliams[8], Nozomu Nishitani[9]

1. Department of Astronomy and Center for Space Physics, Boston University, Massachusetts, USA
2. Cooperative Programs for the Advancement of Earth System Science, University Corporation for Atmospheric Research, Boulder, Colorado, USA
3. Department of Mechanical Engineering and Center for Space Physics, Boston University, Boston, Massachusetts, USA
4. Department of Electrical and Computer Engineering and Center for Space Sciences, Boston University, Boston, Massachusetts, USA
5. Department of Atmospheric and Oceanic Sciences, University of California, Los Angeles, California, USA
6. Department of Earth, Planetary and Space Sciences, University of California, Los Angeles, California, USA
7. The Bradley Department of Electrical and Computer Engineering, Virginia Tech, Blacksburg, Virginia, USA
8. Institute of Space and Atmospheric Studies, University of Saskatchewan, Saskatoon, Saskatchewan, Canada
9. Center for International Collaborative Research, Institute for Space-Earth Environmental Research, Nagoya University, Nagoya, Japan

Corresponding author: Ying Zou

1. Department of Astronomy and Center for Space Physics, Boston University, Massachusetts, USA

2. Cooperative Programs for the Advancement of Earth System Science, University Corporation for Atmospheric Research, Boulder, Colorado, USA

yingzou@bu.edu

Keyword: 2784 Solar wind–magnetosphere interactions; 2724 Magnetopause, cusp, and boundary layers; 7835 Magnetic reconnection

Abstract

Magnetic reconnection can vary considerably in spatial extents. At the Earth's magnetopause, the extent generally corresponds to the extent in local time. The extent has been probed by multi-spacecraft crossing the magnetopause, but the estimates have large uncertainties because of the assumption of spatially continuous reconnection activity between spacecraft and the lack of information beyond areas of spacecraft coverage. The limitations can be overcome by using radars examining ionospheric flows moving anti-sunward across the open-closed field line boundary. We therefore infer the extents of reconnection using coordinated observations of multi-spacecraft and radars for three conjunction events. We find that when reconnection jets occur at only one spacecraft, only the ionosphere conjugate to this spacecraft shows a channel of fast anti-sunward flow. When reconnection jets occur at two spacecraft and the spacecraft are separated by <1 Re, the ionosphere conjugate to both spacecraft shows a channel of fast anti-sunward flow. The consistency allows us to determine the reconnection jet extent by measuring the ionospheric flows. The full-width-at-half-maximum flow extent is 200, 432, and 1320 km, corresponding to a reconnection jet extent of 2, 4, and 11 Re. Considering that reconnection jets emanate from reconnection of a high reconnection rate, the result indicates that both spatially patchy (a few Re) and spatially continuous and extended reconnection (>10 Re) are possible forms of active reconnection at the magnetopause. Interestingly, the extended reconnection develops from a localized patch via spreading across local time. Potential effects of IMF Bx and By on the reconnection extent are discussed.

1. Introduction

A long-standing question in magnetic reconnection is what is the spatial extent of reconnection in the direction normal to the reconnection plane. At the Earth's magnetopause, for a purely southward IMF, this corresponds to the extent in the local time or azimuthal direction. The extent of reconnection has significant relevance to solar wind-magnetosphere coupling, as it controls the amount of energy being passed through the boundary from the solar wind into the magnetosphere and ionosphere. Magnetopause reconnection tends to occur at sites of strictly anti-parallel magnetic fields as anti-parallel reconnection [e.g. *Crooker,* 1979; *Luhmann et al.*, 1984], or occur along a line passing through the subsolar region as component reconnection [e.g. *Sonnerup,* 1974; *Gonzalez and Mozer*, 1974]. Evidence shows either or both can occur at the magnetopause, and the overall reconnection extent can span from a few to 40 Re [*Paschmann et al.*, 1986; *Gosling et al.*, 1990; *Phan and Paschmann*, 1996; *Coleman et al.*, 2001; *Phan et al.*, 2001, 2003; *Chisham et al.*, 2002, 2004, 2008; *Petrinec and Fuselier*, 2003; *Fuselier et al.*, 2002, 2003, 2005, 2010; *Pinnock et al.*, 2003; *Bobra et al.*, 2004; *Trattner et al.*, 2004, 2007, 2008, 2017; *Trenchi et al.*, 2008]. However, reconnection does not occur uniformly across this configuration but has spatial variations [*Pinnock et al.*, 2003; *Chisham et al.*, 2008], and it is the reconnection of high reconnection rates that effectively contributes to the momentum and energy flow within the magnetosphere. Reconnection of high reconnection rates is expected to cause rapid magnetic flux generation and fast reconnection jets. This paper therefore investigates the spatial extent of reconnection through the extents of reconnection jets.

Numerical models show that reconnection tends to occur at magnetic separators, i.e. at the

junction between regions of different magnetic field topologies, and global MHD models have identified a spatially continuous separator along the magnetopause [*Dorelli et al.*, 2007; *Laitinen et al.*, 2006, 2007; *Haynes and Parnell*, 2010; *Komar et al.*, 2013; *Glocer et al.*, 2016]. However, little is known about where and over what range along the separators reconnection proceeds at a high rate. Reconnection in numerical simulations can be activated by introducing perturbations of the magnetic field or can grow spontaneously with instability or resistivity inherent in the system [e.g. *Hesse et al.*, 2001; *Scholer et al.*, 2003]. When reconnection develops as patches (as due to the instabilities or localized perturbations), the patches can spread in the direction out of the reconnection plane [*Huba and Rudakov*, 2002; *Shay et al.* 2003; *Lapenta et al.*, 2006; *Nakamura et al.*, 2012; *Shepherd and Cassak*, 2012; *Jain et al.*, 2013]. The patches either remain patchy after spreading if the current layer is thick, or form an extended X-line if the current layer is already thin [*Shay et al.*, 2003].

Studies have attempted to constrain the extent of reconnection based on fortuitous satellite conjunctions where the satellites detect reconnection jets at the magnetopause at different local times nearly simultaneously [*Phan et al.*, 2000, 2006; *Walsh et al.*, 2014a, 2014b, 2017]. The satellites were separated by a few Re in *Phan et al.* [2000] and *Walsh et al.* [2014a, 2014b, 2017], and >10 Re in *Phan et al.* [2006], and this is interpreted as the reconnection being active over a few Re and even 10 Re, respectively. At the magnetopause, reconnection of a few Re is often referred to as spatially patchy [e.g., *Fear et al.*, 2008, 2010], and reconnection of >10 Re is spatially extended [*Dunlop et al.*, 2011; *Hasegawa et al.*, 2016]. The term patchy has also been used to describe the temporal characteristics of reconnection [e.g. *Newell and Meng*, 1991]. But this paper primarily focuses on the spatial properties. The extent has been alternatively determined by studying the structures of newly reconnected flux tubes, i.e., flux transfer events (FTEs) [*Russell*

116 *and Elphic*, 1978; *Haerendel et al.*, 1978]. Conceptual models regard FTEs either as azimuthally
117 narrow flux tubes that intersect the magnetopause through nearly circular holes, as formed by
118 spatially patchy reconnection [*Russell and Elphic*, 1978], or as azimuthally elongated bulge
119 structures or flux ropes that extend along the magnetopause, as formed by spatially extended
120 reconnection [*Scholer*, 1988; *Southwood et al.*, 1987; *Lee and Fu*, 1985]. FTEs have been
121 observed to be on the order of a few Re wide in local time [*Fear et al.*, 2008, 2010; *Wang et al.*,
122 2005, 2007]. FTEs have also been observed across ~20 Re from the subsolar region to the flanks
123 [*Dunlop et al.*, 2011]. But it is unclear whether these FTEs are branches of one extended bulge or
124 flux rope, or multiple narrow tubes formed simultaneously. When the satellites are widely spaced,
125 it is in general questionable whether a reconnection jet/FTE is spatially continuous between the
126 satellites or whether satellites detect the same moving reconnection jet/FTE. Satellites with a small
127 separation may possibly measure the same reconnection jet/FTE, but only provide a lower limit
128 estimate of the extent. A reconnection jet/FTE may also propagate or spread between satellite
129 detection but satellite measurements cannot differentiate the spatial and temporal effects.
130 This situation can be improved by studying ionospheric signatures of reconnection and FTEs,
131 since their spatial sizes in the ionosphere can be obtained from wide field ground instruments or
132 Low-Earth orbit spacecraft. The ionospheric signatures include poleward moving auroral forms
133 (PMAFs), channels of flows moving anti-sunward across the open-closed field line boundary [e.g.,
134 *Southwood*, 1985], and cusp precipitation [*Lockwood and Smith*, 1989, 1994; *Smith et al.*, 1992].
135 Radar studies have shown that the flows can differ considerably in size, varying from tens of km
136 [*Oksavik et al.*, 2004, 2005], to hundreds of km [*Goertz et al.*, 1985; *Pinnock et al.*, 1993, 1995;
137 *Provan and Yeoman*, 1999; *Thorolfsson et al.*, 2000; *McWilliams et al.*, 2001a, 2001b], and to
138 thousands of km [*Provan et al.*, 1998; *Nishitani et al.*, 1999; *Provan and Yeoman*, 1999]. A

similarly broad distribution has been found for PMAFs [e.g. *Sandholt et al.*, 1986, 1990; *Lockwood et al.*, 1989, 1990; *Milan et al.*, 2000, 2016] and the cusp [*Crooker et al.*, 1991; *Newell and Meng*, 1994; *Newell et al.*, 2007]. This range of spatial sizes in the ionosphere approximately corresponds to a range from <1 to >10 Re at the magnetopause. However, care needs to be taken when interpreting the above ionospheric features, since they could also form due to other drivings such as solar wind dynamic pressure pulses [*Lui and Sibeck*, 1991; *Sandholt et al.*, 1994]. An unambiguous proof of their connection to magnetopause reconnection requires simultaneous space-ground coordination [*Elphic et al.*, 1990; *Denig et al.*, 1993; *Neudegg et al.*, 1999, 2000; *Lockwood et al.*. 2001; *Wild et al.*, 2001, 2005, 2007; *McWilliams et al.*, 2004; *Zhang et al.*, 2008].

Therefore a reliable interpretation of reconnection extent has been difficult due to observation limitations. We will address this by comparing the extents probed by multi-spacecraft and radars using space-ground coordination. On one hand, this enables us to investigate whether reconnection spans continuously between satellites, and how wide reconnection extends beyond satellites. On the other hand, this helps to determine whether reconnection is the driver of ionospheric disturbances and whether the in-situ extent is consistent with the ionospheric disturbance extent.

2. Methodology

We study the local time extent of reconnection jets as a characteristic extent of reconnection. We use conjugate measurements between the Time History of Events and Macroscale Interactions during Substorms (THEMIS) [*Angelopoulos*, 2008] and Super Dual Auroral Network (SuperDARN) [*Greenwald et al.*, 1995]. We focus on intervals when the IMF in OMNI data remains steadily southward. We require that two of the THEMIS satellites fully cross the magnetopause nearly simultaneously and that the satellite data provide clear evidence for

reconnection occurring or not. The full crossings are identified by a reversal of the Bz magnetic field and a change in the ion energy spectra. The requirements of nearly simultaneous crossings and steady IMF conditions help to reduce the spatial-temporal ambiguity by satellite measurements, where the presence/absence of reconnection jets at different local times likely reflects spatial structures of reconnection. Reconnection can still possibly vary between the two satellite crossings, and we use the radar measurements to examine whether the reconnection of interest has continued to exist and maintained its spatial size.

Identification of reconnection jets in the magnetosphere is based on the fluid (MHD) evidence of magnetopause reconnection. Reconnection accelerates plasma bulk flow to Alfvenic speed producing reconnection jets at the magnetopause, and the acceleration should be consistent with the prediction of tangential stress balance across a rotational discontinuity, i.e. Walen relation [*Hudson*, 1970; *Paschmann et al.*, 1979]. The Walen relation is expressed as

$$\Delta V_{predicted} = \pm(1-\alpha_1)^{1/2}(\mu_o\rho_1)^{-1/2}[B_2(1-\alpha_2)/(1-\alpha_1) - B_1] \qquad (1)$$

Where ΔV is the change in the plasma bulk velocity vector across the discontinuity. B and ρ are the magnetic field vector and plasma mass density. μ_0 is the vacuum permeability. $\alpha = (p_{\parallel} - p_{\perp})\mu_0/B^2$ is the anisotropy factor where $p_{\parallel}$ and $p_{\perp}$ are the plasma pressures parallel and perpendicular to the magnetic field. The magnetic field and plasma moments are obtained from the fluxgate magnetometer (FGM) [*Auster et al.*, 2008] and the ElectroStatic Analyzers (ESA) instrument [*McFadden et al.*, 2008]. The plasma mass density is determined using the ion number density, assuming a mixture of 95% protons and 5% helium. The subscripts 1 and 2 refer to the reference interval in the magnetosheath and to a point within the magnetopause, respectively. The magnetosheath reference interval is a 10-s time period just outside the magnetopause. The point within the magnetopause is taken at the maximum ion velocity change across the magnetopause.

We ensure that the plasma density at this point is >20% of the magnetosheath density to avoid the slow-mode expansion fan [*Phan et al.*, 1996]. We compare the observed ion velocity change with the prediction from the Walen relation. The level of agreement is measured by $\Delta V^* = \Delta V_{obs} \cdot \Delta V_{predicted} \Big/ |\Delta V_{predicted}|^2$, following *Paschmann et al.* [1986]. Here $\Delta Vobs$ is the observed ion velocity change. By convention only the velocity changes with $\Delta V^* > 0.5$ are classified as reconnection jets [e.g., *Phan et al.*, 1996; 2013]. To further ensure that reconnection occurs, we examine the kinetic signature of reconnection, which is D-shaped ion distributions at the magnetopause. As magnetosheath ions encounter newly opened magnetic field lines at the magnetopause, they either transmit through the magnetopause entering the magnetosphere or reflect at the boundary. The transmitted ions have a cutoff parallel velocity (i.e. de-Hoffman Teller velocity) below which no ions could enter the magnetosphere. The D-shaped ion distributions are deformed into a crescent shape as ions travel away from the reconnection site [Broll et al. 2017]. We require the satellites to operate in the Fast Survey or Burst mode in which ion distributions are available at 3 s resolution.

We determine reconnection being active if the plasma velocity change across the magnetopause is consistent with the Walen relation with ΔV^* >= 0.5, and if the ions at the magnetopause show a D shape distribution. Reconnection is deemed absent if neither of the two signatures is detected. We require that at least one of the two satellites observe reconnection signatures. Reconnection is regarded as ambiguous if only one of the two signatures is detected, and such reconnection is excluded from our analysis.

We mainly use the three SuperDARN radars located at Rankin Inlet (RKN, geomagnetic 72.6° MLAT, -26.4° MLON), Inuvik (INV, 71.5° MLAT, -85.1° MLON), and Clyde River (CLY, 78.8° MLAT, 18.1° MLON) to measure the ionospheric convection near the dayside cusp. The three

radars have overlapping field of views (FOVs), enabling a reliable determination of the 2-d convection velocity. The FOVs cover the ionosphere >75° MLAT, covering the typical location of the cusp under weak and modest solar wind driving conditions [i.e., *Newell et al.*, 1989] and the high occurrence region of reconnection-related ionospheric flows [*Provan and Yeoman*, 1999] with high spatial resolution. Data from Saskatoon (SAS, 60° MLAT, -43.8° MLON) and Prince George (PGR, 59.6° MLAT, -64.3° MLON) radars are also used when data are available. The measurements of these two radars at far range gates can overlap with the cusp. The radar data have a time resolution of 1-2 min. We focus on observations ±3 h MLT from magnetic noon (approximately 1600-2200 UT). The satellite footprints should be mapped close to the radar FOVs under the Tsyganenko (T89) model [*Tsyganenko*, 1989]. Footprints mapped using different Tsyganenko (e.g., T96 or T01 [*Tsyganenko*, 1995, 2002a, 2002b]) models have similar longitudinal locations (difference <100 km), implying the longitudinal uncertainty of mapping to be small. The latitudinal uncertainty can be inferred by referring to the open-closed field line boundary as estimated using the 150 m/s spectral width boundary [e.g., *Baker et al.*, 1995, 1997; *Chisham and Freeman*, 2003]. And T89 has given the smallest latitudinal uncertainty for the studied events. We surveyed years 2014-2016 during the months when the satellite apogee was on the dayside, and present three events in the paper.

The ionospheric signature of reconnection jets includes fast anti-sunward flows moving across the open-closed field line boundary. We obtain the flow velocity vectors by merging line-of-sight (LOS) measurements at the radar common FOVs [*Ruohoniemi and Baker*, 1998], and these merged vectors reflect the true ionospheric convection velocity. However, the radar common FOVs are hundreds of km wide only, which can be too small to cover the full azimuthal extent of the reconnection-related flows (which are up to thousands of km wide). We therefore also reconstruct

231 the velocity field using the Spherical Elementary Current Systems (SECS) method [*Amm et al.*,
232 2010]. Similar to the works by *Ruohoniemi et al.* [1989] and *Bristow et al.* [2016], the SECS
233 method reconstructs a divergence-free flow pattern using all LOS velocity data. We refer to these
234 velocities as SECS velocities. The accuracy of SECS velocities can be validated by comparing to
235 the LOS measurements and the merged vectors. SECS velocities work best in regions with dense
236 echo coverage and those around sparse echoes are not reliable and thus are excluded from our
237 analysis.

238 The third way of obtaining a velocity field is Spherical Harmonic Fit (SHF). This method uses
239 the LOS measurements and a statistical convection model to fit the distribution of electrostatic
240 potential, which is expressed as a sum of spherical harmonic functions [*Ruohoniemi and Baker*,
241 1998]. The statistical model employed here is *Cousins and Shepherd* [2010]. While this method
242 may suppress small or meso-scale velocity details, such as, sharp flow gradients or flow vortices,
243 we compare SHF velocities with the LOS measurements and merged vectors to determine how
244 well the SHF velocities depict the velocity details.

245 As seen in our observations presented below, the longitudinal profile of the fast anti-sunward
246 ionospheric flows has a near bell shaped curve. We measure the extent based on full width at half
247 maximum (FWHM) of the profile at 1° poleward of the open-closed field line boundary. The
248 choice of FWHM is analogous to *Shay et al.* [2003], where the reconnection extent is measured as
249 regions of electron speed above half of the peak electron flow speed during reconnection. The
250 choice is also supported by magnetopause observations, where we find that ionospheric flows with
251 a speed above half of the peak flow speed map to jets consistent with Walen relation, while those
252 with a speed below map to jets much slower than the Walen relation (Section 3.1). However, it
253 should be noted that the magnitude of the widths is always dependent on the threshold used, and

254 that half maximum is very likely not the only sensible threshold. Using FWHM excludes
255 ionospheric flows with a speed below half of the peak flow speed. Those flows, if related to
256 reconnection, associate with comparatively slow generation of open magnetic flux and low
257 contribution to geomagnetic activity.

258 Among the three presented events, the time separations of magnetopause crossings by two
259 satellites are 1, 2, and 30 min. While the time separation for the third case is somewhat long, we
260 distinguish the spatial and temporal effects using the radar data. Although the three events occurred
261 under similar IMF Bz conditions, the reconnection-related flows in the ionosphere had an
262 azimuthal extent varying from a few hundred km (Sections 3.1-3.2) to more than a thousand km
263 wide (Section 3.3). This corresponds to reconnection of a few to >10 Re wide indicating that both
264 spatially patchy (a few Re) and spatially continuous and extended reconnection (>10 Re) are
265 possible forms of active reconnection at the magnetopause. Interestingly, the extended
266 reconnection was found to arise from a spatially localized patch that spreads azimuthally. Potential
267 effects of IMF Bx and By on the reconnection extent are discussed in Section 4.

268 Note that reconnection can happen over various spatial and temporal scales and our space-
269 ground approach can resolve reconnection that are larger than 0.5 Re and persist longer than a few
270 minutes. This is limited by the radar spatial and temporal resolution, and the magnetosphere-
271 ionosphere coupling time which is usually 1-2 min [e.g. *Carlson et al.*, 2004]. This constraint is
272 not expected to impair the result because reconnection above this scale has been found to occur
273 commonly in statistics (see the Introduction section for spatial and *Lockwood and Wild* [1993],
274 *Kuo et al.* [1995], *Fasel* [1995], and *McWilliams et al.* [1999] for temporal characteristics).

275

276 3. Observations

3.1. Spatially patchy reconnection active at one satellite only

3.1.1 In-situ satellite measurements

On February 2, 2013, THA and THE made simultaneous measurements of the dayside magnetopause with a 1.9 Re separation in the Y direction around 21:25 UT. The IMF condition is displayed in Figure 1a and the IMF was directed southward. The satellite location in the GSM coordinates is displayed in Figure 1b, and the measurements are presented in Figure 2. The magnetic field and the ion velocity components are displayed in the LMN boundary normal coordinate system, where *L* is along the outflow direction, *M* is along the X-line, and *N* is the current sheet normal. The coordinate system is obtained from the minimum variance analysis of the magnetic field at each magnetopause crossing [*Sonnerup and Cahill*, 1967]. Figures 2g-p show that both satellites passed from the magnetosheath into the magnetosphere, as seen as the sharp changes in the magnetic field, the ion spectra, and the density (shaded in pink).

As THE crossed the magnetopause boundary layer (2122:57-2123:48 UT), it detected a rapid, northward-directed plasma jet within the region where the magnetic field rotated (Figures 2g and 2j). The magnitude of this jet relative to the sheath background flow reached 262 km/s at its peak, which was 72% of the predicted speed of a reconnection jet by the Walen relation (366 km/s, not shown). The angle between the observed and predicted jets was 39°. THE also detected kinetic signatures of reconnection. The ion distributions in Figure 2k showed a distorted D-shaped distribution similar to the finding of by *Broll et al.* [2018]. The distortion is due to particles traveling in the field-aligned direction from the reconnection site to higher magnetic field region, and *Broll et al.* [2018] estimated the traveling distance to be a few Re for the observed level of distortion.

THA crossed the magnetopause one to two minutes later than THD (2124:48-2125:13 UT).

While it still identified a plasma jet at the magnetopause (Figures 2l and 2o), the jet speed was significantly smaller than what was predicted for a reconnection jet (80 km/s versus 380 km/s in the *L* direction). The observed jet was directed 71° away from the prediction. The ion distributions deviated from clear D-shaped distributions (Figure 2p). This suggests that the reconnection jet at THE likely did not extend to THA.

3.1.2 Ground radar measurements

The velocity field of the dayside cusp ionosphere during the satellite measurements is shown in Figures 2a-c. Figure 2a shows the radar LOS measurements at 21:25 UT, as denoted by the color tiles, and the merged vectors, as denoted by the arrows. The colors of the arrows indicate the merged velocity magnitudes, and the colors of the tiles indicate the LOS speeds that direct anti-sunward (those project to the sunward direction appear as black). Fast (red) and anti-sunward flows are the feature of our interest. One such of this flow can be identified in the pre-noon sector, which had a speed of ~800 m/s and was directed poleward and westward. As the merged vector arrows indicate, the velocity vectors have a major component close to the INV beam directions and thus the INV LOS velocities reflect the flow distribution. The flow crossed the open-closed field line boundary, which was located at 78° MLAT based on the spectral width (Figure 2d and S1). This flow thus meets the criteria of being an ionospheric signature of magnetopause reconnection jets. Another channel of fast flow was present in the post-noon sector. This post-noon flow was directed more azimuthally and was increasingly separated from the pre-noon flow as it moved away from the noon (see the region of slow velocities at >79° MLAT around noon). The difference in flow trajectories implies that these flows were driven by different magnetic tension forces. They also evolved differently over time as seen in Figure 2e which is discussed below. The flows thus likely

originated from two reconnection regions that were associated with different magnetic field topologies and different temporal variabilities. Since the satellites were located in the pre-noon sector we focus on the pre-noon flow below.

The flow had a limited azimuthal extent. The extent is determined at half of the maximum flow speed, which was ~400 m/s. Figure 2f discussed below shows a more quantitative estimate of the extent. In Figure 2a, we mark the eastern and western boundaries with the dashed magenta lines, across which the LOS velocities dropped from red to blue/green colors.

Figure 2b shows the SECS velocities, denoted by the arrows. The SECS velocities reasonably reproduced the spatial structure of the flows seen in Figure 2a. The flow boundaries were marked by the dashed magenta lines, across which the flow speed dropped from red to blue. Across the flow western boundary the flow direction also reversed. The equatorward-directed flows are interpreted as the return flow of the poleward flows, as sketched in *Southwood* [1987] and *Oksavik et al.* [2004].

The velocity field reconstructed using the SHF velocities is shown in Figure 2c (obtained through the Radar Software Toolkit (http://superdarn.thayer.dartmouth.edu/software.html)). This is an expanded view of the global convection maps in Figure S2 focusing on the dayside cusp. Comparing Figures 2c and S2 reveals that the employed radars listed in Section 2 have contributed to the majority of the backscatters on the dayside. This is because this event (same for the following two events) occurred under non-storm time, where the open-closed field line was confined within the FOVs of the radars used. During storm time the boundary expands to lower latitude where backscatter from a wider network of radars may be available. The SHF velocities also captured the occurrence of two flows in the pre- and post-noon sectors, respectively, although the orientation of the flows were slightly different from Figure 2a or 2b. The difference is likely due to the

346 contribution from the statistical potential distribution under the southward IMF. The flow western
347 and eastern boundaries were again marked by the dashed magenta lines.
348 Figure 2d shows spectral width measurements. Large spectral widths can be produced by soft
349 (~100 eV) electron precipitation [*Ponomarenko et al.*, 2007], and evidence has shown that the
350 longitudinal extent of large spectral widths correlates with the extent of PMAFs [*Moen et al.*, 2000]
351 and of poleward flows across the open-closed field line boundary [*Pinnock and Rodger*, 2001].
352 Large spectral widths thus have the potential to reveal the reconnection extent. For the specific
353 event under examination, the region of large spectral widths, appearing as red color, spanned from
354 10.5 to 14.5 h MLT if we count the sporadic scatters in the post-noon sector. This does not
355 contradict the flow width identified above because the wide width reflects the summed width of
356 the pre- and post-noon flows. In fact a more careful examination shows that there might exist two
357 dark red regions (circled in red, the red dashed line is due to the discontinuous backscatters outside
358 the INV FOV) embedded within the ~200-m/s spectral widths. These two regions had slightly
359 higher spectral widths than the surrounding (by ~20-50 m/s) and possibly corresponded to the two
360 flows.
361 Figures 2a-c all observed a channel of fast anti-sunward flow in the pre-noon sector of the high
362 latitude ionosphere, and the flow had a limited azimuthal extent. If the flow corresponded to a
363 magnetopause reconnection jet, the reconnection jet is expected to span over a limited local time
364 range. This is consistent with the THEMIS satellite observation in Section 3.1.1, where THE at Y
365 = -2.9 Re detected a clear reconnection jet, while THA at Y = -4.8 Re did not. In fact, if we project
366 the satellite location to the ionosphere through field line tracing under the T89 model, THE was
367 positioned at the flow longitude, while THA was to the west of the flow embedded in weak
368 convection (Figure 2a).

While this paper primarily focuses on the spatial extent of reconnection, the temporal evolution can be obtained from the time series plot in Figure 2e. Figure 2e presents the northward component of the SECS velocity along 79° MLAT (just 1° poleward of the open-closed field line boundary) as functions of magnetic local time (MLT) and time. Here we only show the northward component of the SECS velocity as this component represents reconnecting flows across an azimuthally-aligned open-closed field line boundary. Similar to the snapshots, the flow of our interest appears as a region of red color. The time and the location where THA and THE crossed the magnetopause are marked by the crosses. The pre-noon flow emerged from a weak background from 2122 UT and persisted for ~>30 min, while the post-noon flow only lasted for ~10 min. Minutes following the onset the pre-noon flow spread in width, where the western boundary of the red color moved from 10.7 to 10.5 h MLT, and the eastern boundary moved to 11.2 to 11.5 h MLT. After 2134 UT the spreading ceased and the entire flow moved westward (the western boundary moved beyond the ROV). Hence the reconnection-related ionospheric flow, once formed, has spread in width and displaced westward. The spreading behavior is similar to events studied by Zou et al. [2018], and is interpreted to relate to spreading of the reconnection extent seen in simulation studies (see introduction). The spreading has also been noticed in the other two events (see Section 3.3), indicating that this could be a common development feature of the reconnection-related flows.

A consequence of the flow temporal evolution is that THA, which was previously outside the reconnection-related flow, became immersed in the flow from 2130 UT, while THE, which was previously inside the flow, was left outside from 2142 UT (Figure 2e). This implies that at the magnetopause the reconnection has spread azimuthally sweeping across THA, and has slid in the –y direction away from THE. This is in perfect agreement with satellite measurements shown in Figures 2q-z. Figures 2q-z presents subsequent magnetopause crossings made by THA and THE

following the crossings in Figures 2g-p. THA detected an Alfvenic reconnection jet and a clear D-shape ion distribution, and THE detected a jet much slower than the Alfvenic speed and an ion distribution without a clear D-shape. This corroborates the connection between the in-situ reconnection jet with the fast anti-sunward ionospheric flow, and reveals the dynamic evolution of reconnection in the local time direction. On the other hand, this also sheds light on the nature of the slow convection outside the fast flow, which corresponds to sub-Alfvenic jets at the magnetopause.

We quantitatively determine the flow extent in Figure 2f. Figure 2f shows the profile of the northward component of the SECS velocity at 2129 UT as a function of the distance from magnetic noon. The 2129 UT is the time when the flow extent has slowed down from spreading and stabilized. The profile should theoretically be taken just poleward of the open-closed field line boundary. In practice we smooth the velocity in latitude with a 1° window and take measurements 1° poleward of the open-closed field line boundary. The profile has a near bell shaped curve, and the FWHM was 200 km at an altitude of 250 km. Also shown is the INV LOS velocity profile, which is obtained in a similar manner as the SECS one. The LOS velocity profile also gives a narrow FWHM, which was 280 km.

While it is commonly assumed that the extent of reconnection jets reflects the extent of reconnection, we test the assumption by calculating the distribution of reconnection electric field in Figure 3. Reconnection electric field can be estimated by measuring the flow across the open-closed field line boundary in the reference frame of the boundary [*Pinnock et al.*, 2003; *Freeman et al.*, 2007; *Chisham et al.*, 2008], and we follow this procedure to derive the its distribution across local time. A close-up presentation of the open-closed field line boundary is shown in Figures 3a-c around the space-ground conjunction time and longitude. The open-closed field line boundary,

415 drawn as the dashed black line, is identified following *Chisham and Freeman* [2003, 2004] and
416 *Chisham et al.* [2004b, 2005a, 2005b, 2005c]. The boundary was almost along a constant magnetic
417 latitude. The motion of the boundary is obtained by inspecting the time series of the spectral width
418 measurements along each radar beam and examples are given for INV beams 4, 7, and 10 in
419 Figures 3d-f. Subtracting the speed of the boundary from that of the flow (in the rest frame) across
420 the boundary gives the flow speed in the reference frame of the boundary. Assuming that the flow
421 is E × B drift, electric field can be derived and this is the ionosphere-mapped reconnection electric
422 field. The flow speed across the boundary is taken from the 1°-averaged speed at the boundary
423 latitude (similar to *Chisham et al.* [2008]). Note that a precise determination of the boundary
424 motion could be subject to radar spatial and temporal resolution and the error can be as large as
425 300 m/s or 15 mV/m.

426 As shown in Figure 3g, the profile of the reconnection electric field had a peak in the azimuthal
427 direction with a limited FWHM, and the FWHM is essentially the same as the flow width just
428 poleward of the boundary (difference being less than the radar spatial resolution) This establishes
429 the relation between our measure of the reconnection jet extent and the extent of reconnection of
430 high reconnection rates. Regions of high reconnection rates are localized, although those of low
431 reconnection rates (>0 mV/m) can extend over a much broader region. For example, the western
432 boundary of non-zero reconnection rates was located just at the edge of INV FOV (considering
433 the 15 mV/m uncertainty), and the eastern edge extended beyond INV FOV, likely into where the
434 post-noon flow was originated from. A lower estimate of the extent of non-zero reconnection rates
435 is therefore ~4 h MLT. It is likely that there were two components of reconnection at different
436 scales: broad and low-rate background reconnection, and embedded high-rate reconnection.

437 To infer the reconnection extent at the magnetopause, we project the flow extent based on the

SECS in the ionosphere to the equatorial plane. The result suggests that the reconnection local time extent was ~2 Re.

3.2. Spatially patchy reconnection active at both satellites

3.2.1. In-situ satellite measurements

On April 19, 2015, under a southward IMF (Figure 4a), THA and THE crossed the magnetopause nearly simultaneously (<2 min lag) with a 0.5 Re separation in Y (Figure 4b). They passed from the magnetosheath into the magnetosphere. Both satellites observed jets in the V_L component at the magnetopause (Figures 5g-p). The jet at THA at ~1828:05 UT had a speed of 84% of and an angle within ~15° from the Walen prediction. The jet at THE at ~1826:25 UT had a speed of 95% of and an angle of ~29° from the Walen prediction. The ion distributions at THA and THE exhibit clear D-shaped distributions. Reconnection thus occurred at both local times.

Section 3.2.2. Ground radar measurements

During the satellite measurements, the radars observed a channel of fast anti-sunward flow around magnetic noon (Figures 5a-c). The flow crossed the open-closed field line boundary at 77° MLAT, and qualifies for an ionospheric signature of magnetopause reconnection jets. The flow direction was nearly parallel to the RKN radar beams, and therefore the RKN LOS measurements in Figure 5a approximated to the 2-d flow speed. The flow eastern boundary can be identified as where the velocity dropped from red/orange to blue (dashed magenta line). Determining the flow western boundary requires more measurements of the background convection velocity, which is beyond the RKN FOV. But we infer that the western boundary did not extend more than 1.5 h westward beyond the RKN FOV because the PGR and INV echoes there showed weakly poleward

and equatorward LOS speeds around the open-closed field line boundary. The CLY radar data further indicated that the anti-sunward flow had started to rotate westward immediately beyond the RKN FOV. This is because the CLY LOS velocities measured between the RKN and INV radar FOVs were larger for more east-west oriented beams (appearing as yellow color) than for more north-south oriented beams (green color). The rotation likely corresponds to the vortex at the flow western boundary as sketched in *Oksavik et al.* [2004].

The more precise location of the western boundary can be retrieved from the SECS velocities in Figure 5b and the SHF velocities in Figure 5c. The SECS velocities present a flow channel very similar to that in Figure 5a, while the flow channel in the SHF velocities was more azimuthally-aligned than in Figures 5a-b.

The determined flow extent agrees with the extent of the cusp in Figure 5d. The high spectral widths associated with the cusp were located at the western half of the RKN FOV. They extended westward beyond the RKN FOV into CLY far range gates, where they dropped from red to green color. This is consistent with the inferred location and extent of the anti-sunward flow.

The flow of our interest just emerged from a weak background at the time when the THEMIS satellites crossed the magnetopause (Figure 5e). This implies that the related reconnection just activated at the studied local time. The flow spread azimuthally until 1833 UT when it stabilized. We quantify the stabilized flow extent and the reconnection electric field extent (Figure 5f) in a similar way as Figure 2f and Figure 3g. The FWHM of the flow is determined to be 432 and 336 km based on the SECS and RKN LOS data respectively. While the reconnection electric field had data gaps due to the limited coverage and backscatter availability at near range gate, it implies a western boundary of FWHM consistent with the flow slightly poleward of it. This is also the western boundary of non-zero reconnection rates considering the 15-mV/m uncertainty. The

484 eastern boundary extended beyond RKN FOV. The FWHM of the SECS flow profile corresponds
485 to ~4 Re in the equatorial plane.

486 The fact that the fast anti-sunward flow had a limited azimuthal extent around magnetic noon
487 implies that the corresponding magnetopause reconnection should span over a limited local time
488 range around the noon. This is consistent with the THEMIS satellite observation in Section 3.2.1,
489 where reconnection was active at Y = 0.7 (THA) and 0.2 Re (THE). Projecting THA and THE
490 locations to the ionosphere reveals that both satellite footprints were located within the flow
491 longitudes. Therefore the reconnection at the two satellites was part of the same reconnection
492 around the subsolar point of the magnetopause. (The THE footprint was equatorward of THA
493 because the X location of THE was closer to the Earth than THA. The magnetopause was
494 expanding and it swept across THE and then THA.) The reconnection further extended azimuthally
495 beyond the two satellite locations, reaching a full length of ~4 Re.

496

497 3.3. Spatially continuous and extended reconnection active at both satellites

498 3.3.1. In-situ satellite measurements

499 On Apr 29, 2015, under a prolonged and steady southward IMF (Figure 6a), THA and THE
500 crossed the magnetopause successively with a time separation of ~30 min. The locations of the
501 crossings were separated by 0.1-0.2 Re in the Y direction (Figure 6b). The satellites passed from
502 the magnetosphere into the magnetosheath, and the magnetic field data suggest that the satellites
503 crossed the current layer multiple times before completely entering the magnetosheath (Figures
504 6i-r). We therefore only display the magnetic field and the plasma velocity in the GSM coordinates.
505 Both satellites detected multiple flow jets, all agreeing with the Walen prediction with $\Delta V^* > 0.5$.
506 For example, the jet at 1849-1850 UT measured by THA had a speed with 80% of and angle with

9° from the Walen prediction, and the jet at 1920-1922 UT by THE had a speed with 83% of and an angle with 1° from the Walen prediction. The ion distributions at THA and THE exhibit clear D-shaped distributions.

3.3.2. Ground radar measurements

In the ionosphere, the radars detected a fast anti-sunward flow as an ionospheric signature of the magnetopause reconnection jet (Figures 7a-c). The flow had a broad azimuthal extent, as delineated by the dashed magenta lines (Figure 7a). A similar flow distribution is found in the SECS velocities (Figure 7b), and the SHF velocities (Figure 7c). The flow propagated into the polar cap as one undivided channel (as opposed to Section 3.1.2), implying that it was one flow structure at least to the resolution the radars can resolve. Corresponding to the broad extent of the flow, the cusp had a broad extent (Figure 7d). The cusp continuously spanned across the INV and RKN FOVs and its western and eastern edges coincided with the western and eastern boundaries of the flow, supporting our delineation of the flow extent.

The wide flow channel in the ionosphere implies that the corresponding magnetopause reconnection jet should be wide in local time. Based on the flow distribution, we infer that much of the reconnection should be located on the pre-noon sector, except that the eastern edge can extend across the magnetic noon meridian to the early post-noon sector. This inference is again consistent with the inference from the THA and THE measurements that the reconnection extended at least over the satellite separation (Y = -0.2 (THA) and 0 Re (THE)). Note, however, that the distance between THA and THE only covered <2% of the reconnection extent determined from the ionosphere flow. While the satellite configuration and measurements here were similar to those in Section 3.2, the extent of reconnection was fundamentally different. This suggests that it is

difficult to obtain a reliable estimate of the reconnection extent without the support of 2-d measurements and that satellites alone also cannot differentiate spatially extended reconnection from spatially patchy reconnection.

The flow temporal evolution is shown in Figures 7e, where the velocities are the northward component of the SECS data. An overall wide flow channel is seen during the time interval of our interest with the eastern and western boundaries located at ~12.0-12.5 and ~8.0-8.7 h MLT, respectively. But between the two satellite observations, the flow experienced an interesting variation. The velocity at 9.3-12.0 h MLT dropped by 100-200 m/s during 1902-1912 UT (red color turned orange, yellow, and then green), while the velocity at 8.6-9.3 h MLT did not change substantially. The velocity enhanced again from 1912 UT. The enhancement centered at 10.7 h MLT and spread azimuthally towards east and west. The enhancement spread by 0.7 h MLT over 14 min at its eastern end (marked by the dashed black line), suggesting a spreading speed of 275 m/s. The enhancement spread by 1.2 h MLT at its western end, suggesting a spreading speed of 471 m/s. It should be noted that the all three components of the IMF stayed steady for an extended time (Figure 8, discussed below in Section 4), and thus the evolution of the flow/reconnection was unlikely to be externally driven.

This sequence of changes gives an important implication that the spatially extended reconnection was a result of spreading of an initially patchy reconnection. If we map the spreading in the ionosphere to the magnetopause, the spreading occurred bi-directionally and at a speed of 15 and 26 km/s in the east and west directions based on field-line mapping under the T89 model (the mapping factor was 55). Such an observation is similar to what has recently been reported by *Zou et al.* [2018], where the reconnection also spreads bi-directionally at a speed of a few tens of km/s. However, the spreading in *Zou et al.* [2018] occurs following a southward turning of the

553 IMF, while the spreading here occurred without IMF variations. The mechanism of spreading is
554 explained either as motion of the current carriers of the reconnecting current sheet or as
555 propagation of the Alfven waves along the guide field [*Huba and Rudakov*, 2002; *Shay et al.* 2003;
556 *Lapenta et al.*, 2006; *Nakamura et al.*, 2012; *Jain et al.*, 2013].

557 It should be noted that reconnection spreading can be a common process of reconnection that is
558 not limited to extended reconnection. It also occurs for patchy reconnection as seen in Sections 3.1
559 and 3.2. The spreading speeds were similar across the three events but the duration of the spreading
560 process was two to three times longer in the spatially extended than the spatially patchy
561 reconnection events. For the extended reconnection, the spreading process persisted for 14 min
562 expanding the extent by 5-6 Re.

563 Figure 7f quantifies the extent of the flow and reconnection electric field. The FWHM extent
564 was 1320 km based on the SECS data. Despite the presence of the data gaps, the LOS
565 measurements suggest a western and eastern boundary consistent with the SECS data. The
566 reconnection electric field had a similar FWHM to the flow although regions of non-zero
567 reconnection rates again extended beyond the available coverage indicating an overall extent >4 h
568 MLT. The extent corresponds to a reconnection extent of ~11 Re.

569

570 4. Discussion

571 The above events definitely show that the local time extent of magnetopause reconnection can
572 vary from a few to >10 Re. Here we investigate whether and how the extent may depend on the
573 upstream driving conditions. Figure 8 presents the IMF, the solar wind velocity, and the solar wind
574 pressure taken from the OMNI data for the three events. The red vertical lines mark the times when
575 the reconnection was measured. The three events occurred under similar IMF field strengths (5-6

nT), similar IMF Bz components (-2-3 nT), and similar dynamic pressures (1-2 nPa), implying that the different reconnection extents were unlikely due to these parameters. The solar wind speeds had a slight decreasing trend as the reconnection extent increased. This is different from *Milan et al.* [2016], who identified a large solar wind speed as a cause of a large reconnection extent. However, *Milan et al.* [2016] studied reconnection under very strong IMF driving conditions when |B| ~15 nT, while our events occurred under a more typical moderate driving (|B| ~5-6 nT).

The spatially patchy reconnection events had an IMF Bx of a larger magnitude than the extended reconnection event did (4 vs. 0 nT). The spatially patchy reconnection events also had an IMF By component of a smaller magnitude (2 vs. 5 nT, and therefore a clock angle closer to 180°), and with more variability on time scales of tens of minutes, than the extended reconnection event. The IMF Bx and By components are known to modify the magnetic shear across the magnetopause and to affect the occurrence location of reconnection. Studies have found that at dayside low latitude magnetopause small $|B_y|/|B_z|$ relates to anti-parallel and large $|B_y|/|B_z|$ to component reconnection [*Coleman et al.*, 2001; *Chisham et al.*, 2002; *Trattner et al.*, 2007]. Large $|B_x|/|B|$, i.e. cone angle, also favors formation of high-speed magnetosheath jets [*Archer and Horbury*, 2013; *Plaschke et al.*, 2013] of a few Re in scale size, resulting in a turbulent magnetosheath environment for reconnection to occur [*Coleman, and Freeman*, 2005]. The steady IMF condition may allow reconnection to spread across local times unperturbedly, eventually reaching a wide extent. Thus our preliminary analysis suggests that the reconnection extent may depend on the IMF orientation and steadiness, although whether and how they influence the extent needs to be further explored.

5. Summary

We carefully investigate the local time extent of magnetopause reconnection by comparing the measurements of reconnection jets by two THEMIS satellites and three ground radars. When reconnection jets are only observed at one of the two satellite locations, only the ionosphere conjugate to this spacecraft shows a channel of fast anti-sunward flow. When reconnection jets are observed at both spacecraft and the spacecraft are separated by <1 Re, the ionosphere conjugate to both spacecraft shows a channel of fast anti-sunward flow. The fact that the satellite locations are mapped to the same flow channel suggests that the reconnection is continuous between the two satellites, and that it is appropriate to take the satellite separation as a lower limit estimate of the reconnection extent. Whether reconnection can still be regarded as continuous when the satellites are separated by a few or > 10 Re is questionable, and needs to be examined using conjunctions with a larger satellite separation than what have been presented here.

The reconnection extent is measured as the FWHM of the ionospheric flow. In the three conjunction events, the flows have FWHM of 200, 432, and 1320 km in the ionosphere, which corresponds to ~2, 4, and 11 Re at the magnetopause (under the T89 model) in the local time direction. The flow extent is confirmed to be related to reconnection of high reconnection electric field. The result provides strong observational evidence that magnetopause reconnection can occur over a wide range of extents, from spatially patchy (a few Re) to spatially continuous and extended (>10 Re). Interestingly, the extended reconnection is seen to initiate from a patchy reconnection, where the reconnection grows by spreading across local time. The speed of spreading is 41 km/s summing the westward and eastward spreading motion, and the spreading process persists for 14 min broadening the extent by 5-6 Re.

Based on the three events studied in this paper, the reconnection extent may be affected by the IMF orientation and steadiness, although the mechanism is not clearly known. For the observed

622 modest solar wind driving conditions, the spatially extended reconnection is suggested to occur
623 under a smaller IMF Bx component, and a larger and steadier IMF By component than the spatially
624 patchy reconnection. The IMF strength, the Bz component, and the solar wind velocity and
625 pressure are about the same for the extended and the patchy reconnection. This finding, however,
626 could be limited by the number of events under analysis, and further study is needed to achieve an
627 understanding of how solar wind controls reconnection extent. Reconnection can vary with time,
628 even under steady IMF driving conditions.
629
630 **Acknowledgments.** This research was supported by the NASA Living With a Star Jack Eddy
631 Postdoctoral Fellowship Program, administered by UCAR's Cooperative Programs for the
632 Advancement of Earth System Science (CPAESS), NASA grant NNX15AI62G, NSF grants PLR-
633 1341359 and AGS-1451911, and AFOSR FA9550-15-1-0179 and FA9559-16-1-0364. The
634 THEMIS mission is supported by NASA contract NAS5-02099. SuperDARN is a collection of
635 radars funded by national scientific funding agencies. SuperDARN Canada is supported by the
636 Canada Foundation for Innovation, the Canadian Space Agency, and the Province of
637 Saskatchewan. We thank Tomoaki Hori for useful discussion on the SECS technique. Data
638 products of the SuperDARN, THEMIS, and OMNI are available at http://vt.superdarn.org/,
639 http://themis.ssl.berkeley.edu/index.shtml, and GSFC/SPDF OMNIWeb website.
640
641 Reference
642 Amm, O., Grocott, A., Lester, M. and Yeoman, T. K.: Local determination of ionospheric plasma
643 convection from coherent scatter radar data using the SECS technique, J. Geophys. Res., 115,
644 A03304, doi:10.1029/2009JA014832, 2010.

645 Angelopoulos, V.: The THEMIS mission, Space Sci. Rev., 141, 5–34, doi:10.1007/s11214-008-
646 9336-1, 2008.
647 Archer, M. O. and Horbury, T. S.: Magnetosheath dynamic pressure enhancements: occurrence
648 and typical properties, Ann. Geophys., 31, 319-331, https://doi.org/10.5194/angeo-31-319-
649 2013, 2013.
650 Auster, H. U., et al.: The THEMIS fluxgate magnetometer, *Space Sci. Rev.*, **141**, 235–264, 2008.
651 Baker, K. B., Dudeney, J. R., Greenwald, R. A., Pinnock, M., Newell, P. T., Rodger, A. S.,
652 Mattin, N. , and Meng, C.-I.: HF radar signatures of the cusp and low-latitude boundary
653 layer, J. Geophys. Res., 100(A5), 7671–7695, doi:10.1029/94JA01481, 1995.
654 Baker, K. B., Rodger, A. S., and Lu, G.: HF-radar observations of the dayside magnetic merging
655 rate: A Geospace Environment Modeling boundary layer campaign study, J. Geophys.
656 Res., 102(A5), 9603–9617, doi:10.1029/97JA00288, 1997.
657 Bobra, M. G., Petrinec, S. M., Fuselier, S. A., Claflin, E. S., and Spence, H. E.: On the solar
658 wind control of cusp aurora during northward IMF, Geophys. Res. Lett., 31, L04805,
659 doi:10.1029/2003GL018417, 2004.
660 Bristow, W. A., Hampton, D. L., and Otto, A.: High-spatial-resolution velocity measurements
661 derived using Local Divergence-Free Fitting of SuperDARN observations, J. Geophys. Res.
662 Space Physics, 121, 1349–1361, doi:10.1002/2015JA021862, 2016.
663 Chisham, G., Coleman, I. J., Freeman, M. P., Pinnock, M., and Lester, M.: Ionospheric signatures
664 of split reconnection X-lines during conditions of IMF Bz < 0 and |By|/|Bz|: Evidence for the
665 antiparallel merging hypothesis, J. Geophys. Res., 107(A10), 1323,
666 doi:10.1029/2001JA009124, 2002.
667 Chisham, G., and Freeman, M. P.: A technique for accurately determining the cusp-region polar

668 cap boundary using SuperDARN HF radar measurements, Ann. Geophys., 21, 983–996,
669 2003.
670 Chisham, G., Freeman, M. P., Coleman, I. J., Pinnock, M., Hairston, M. R., Lester, M., and
671 Sofko, G.: Measuring the dayside reconnection rate during an interval of due northward
672 interplanetary magnetic field, Ann. Geophys., 22, 4243–4258, 2004.
673 Chisham, G., and M. P. Freeman: An investigation of latitudinal transitions in the SuperDARN
674 Doppler spectral width parameter at different magnetic local times, Ann. Geophys., 22,
675 1187–1202, 2004.
676 Chisham, G., Freeman, M. P., and Sotirelis, T.: A statistical comparison of SuperDARN spectral
677 width boundaries and DMSP particle precipitation boundaries in the nightside ionosphere,
678 Geophys. Res. Lett., 31, L02804, doi:10.1029/2003GL019074, 2004b.
679 Chisham, G., Freeman, M. P., Sotirelis, T., Greenwald, R. A., Lester, M., and Villain J.-P.: A
680 statistical comparison of SuperDARN spectral width boundaries and DMSP particle
681 precipitation boundaries in the morning sector ionosphere, Ann. Geophys., 23,733–743,
682 2005a.
683 Chisham, G., Freeman, M. P., Sotirelis, T., and Greenwald, R. A.: The accuracy of using the
684 spectral width boundary measured in off-meridional SuperDARN HF radar beams as a
685 proxy for the open-closed field line boundary, Ann. Geophys., 23, 2599–2604, 2005b.
686 Chisham, G., Freeman, M. P., Lam, M. M., Abel, G. A., Sotirelis, T., Greenwald, R. A., and
687 Lester, M.: A statistical comparison of SuperDARN spectral width boundaries and DMSP
688 particle precipitation boundaries in the afternoon sector ionosphere, Ann. Geophys., 23,
689 3645–3654, 2005c.
690 Chisham, G., et al.: Remote sensing of the spatial and temporal structure of magnetopause and

691 magnetotail reconnection from the ionosphere, Rev. Geophys., 46, RG1004,
692 doi:10.1029/2007RG000223, 2008.
693 Coleman, I. J., Chisham, G., Pinnock, M., and Freeman, M. P., An ionospheric convection
694 signature of antiparallel reconnection, J. Geophys. Res., 106, 28,995–29,007, 2001.
695 Coleman, I. J., and Freeman, M. P.: Fractal reconnection structures on the magnetopause,
696 Geophys. Res. Lett., 32, L03115, doi:10.1029/2004GL021779, 2005.
697 Cousins, E. D. P., and Shepherd, S. G.: A dynamical model of high‐latitude convection derived
698 from SuperDARN plasma drift measurements, *J. Geophys. Res.*, 115, A12329,
699 doi:10.1029/2010JA016017, 2010.
700 Crooker, N. U., Dayside merging and cusp geometry, J. Geophys. Res., 84(A3), 951–959,
701 doi:10.1029/JA084iA03p00951, 1979.
702 Crooker, N. U., F. R. Toffoletto, and M. S. Gussenhoven, Opening the cusp, J. Geophys.
703 Res., 96(A3), 3497–3503, doi: 10.1029/90JA02099, 1991.
704 Denig, W. F., Burke, W. J., Maynard, N. C., Rich, F. J., Jacobsen, B., Sandholt, P. E., Egeland, S.,
705 Leontjev, A., and Vorobjev, V. G.: Ionospheric signatures of dayside magnetopause
706 transients: A case study using satellite and ground measurements, *J. Geophys.*
707 *Res.*, **98**(A4), 5969–5980, doi:10.1029/92JA01541, 1993.
708 Dorelli, J. C., Bhattacharjee, A., and Raeder, J.: Separator reconnection at Earth's dayside
709 magnetopause under generic northward interplanetary magnetic field conditions, J. Geophys.
710 Res., 112, A02202, doi:10.1029/2006JA011877, 2007.
711 Dunlop, M. W., et al.: Magnetopause reconnection across wide local time, *Ann.*
712 *Geophys.*, **29**, 1683–1697, doi:10.5194/angeo-29-1683-2011, 2011.
713 Elphic, R. C., Lockwood, M., Cowley, S. W. H., and Sandholt, P. E.: Flux transfer events at the

magnetopause and in the ionosphere, Geophys. Res. Lett., 17, 2241, 1990.

Fasel, G. J. (1995), Dayside poleward moving auroral forms: A statistical study, *J. Geophys. Res.*, 100(A7), 11891–11905, doi: 10.1029/95JA00854.

Fear, R. C., Milan, S. E., Fazakerley, A. N., Lucek, E. A., Cowley, S. W. H., and Dandouras, I.: The azimuthal extent of three flux transfer events, Ann. Geophys., 26, 2353-2369, https://doi.org/10.5194/angeo-26-2353-2008, 2008.

Fear, R. C., Milan, S. E., Lucek, E. A., Cowley, S. W. H., and Fazakerley, A. N.: Mixed azimuthal scales of flux transfer events, in *The Cluster Active Archive – Studying the Earth's Space Plasma Environment*, Astrophys. Space Sci. Proc., edited by H. Laakso, M. Taylor, and C. P. Escoubet, pp. 389–398, Springer, Dordrecht, Netherlands, doi:10.1007/978-90-481-3499-1_27, 2010.

Freeman, M. P., G. Chisham, and I. J. Coleman (2007), Remote sensing of reconnection, in Reconnection of Magnetic Fields, edited by J. Birn and E. Priest, chap. 4.6, pp. 217–228, Cambridge Univ. Press, New York.

Fuselier, S. A., Frey, H. U., Trattner, K. J., Mende, S. B., and Burch, J. L.: Cusp aurora dependence on interplanetary magnetic field Bz, J. Geophys. Res., 107(A7), 1111, doi:10.1029/2001JA900165, 2002.

Fuselier, S. A., Mende, S. B., Moore, T. E., Frey, H. U., Petrinec, S. M., Claflin, E. S., and Collier, M. R.: Cusp dynamics and ionospheric outflow, in Magnetospheric Imaging—The Image Mission, edited by J. L. Burch, Space Sci. Rev., 109, 285, doi:10.1023/B:SPAC.0000007522.71147.b3, 2003.

Fuselier, S. A., Trattner, K. J., Petrinec, S. M., Owen, C. J., and Rème, H., Computing the reconnection rate at the Earth's magnetopause using two spacecraft observations, J. Geophys.

737 Res., 110, A06212, doi:10.1029/2004JA010805, 2005.
738 Fuselier, S. A., Petrinec, S. M., and Trattner, K. J.: Antiparallel magnetic reconnection rates at the
739 Earth's magnetopause, J. Geophys. Res., 115, A10207, doi:10.1029/2010JA015302, 2010.
740 Glocer, A., Dorelli, J., Toth, G., Komar, C. M., and Cassak, P. A.: Separator reconnection at the
741 magnetopause for predominantly northward and southward IMF: Techniques and results, J.
742 Geophys. Res. Space Physics, 121, 140–156, doi:10.1002/2015JA021417, 2016.
743 Goertz, C. K., Nielsen, E., Korth, A., Glassmeier, K. H., Haldoupis, C., Hoeg, P.,
744 and Hayward, D.: Observations of a possible ground signature of flux transfer events, J.
745 Geophys. Res., 90(A5), 4069–4078, doi:10.1029/JA090iA05p04069, 1985.
746 Gonzalez, W. D., and Mozer, F. S.: A quantitative model for the potential resulting from
747 reconnection with an arbitrary interplanetary magnetic field, J. Geophys. Res., 79(28), 4186–
748 4194, doi:10.1029/JA079i028p04186, 1974.
749 Gosling, J. T., Thomsen, M. F., Bame, S. J., Onsager, T. G., and Russell, C. T.: The electron edge
750 of low latitude boundary layer during accelerated flow events, Geophys. Res. Lett., 17, 1833–
751 1836, doi:10.1029/GL017i011p01833, 1990b.
752 Greenwald, R. A., et al.: DARN/SuperDARN: A global view of the dynamics of high-latitude
753 convection, Space Sci. Rev., 71, 761–796, 1995.
754 Haerendel, G., Paschmann, G., Sckopke, N., Rosenbauer, H., and Hedgecock, P. C., The frontside
755 boundary layer of the magnetosphere and the problem of reconnection, J. Geophys.
756 Res., 83(A7), 3195–3216, doi:10.1029/JA083iA07p03195, 1978.
757 Hasegawa, H., et al., Decay of mesoscale flux transfer events during quasi‐continuous spatially
758 extended reconnection at the magnetopause, Geophys. Res. Lett., 43, 4755–4762,
759 doi:10.1002/2016GL069225, 2016.

760 Haynes, A. L., and Parnell, C. E., A method for finding three-dimensional magnetic
761 skeletons, *Phys. Plasmas*, **17**, 092903, doi:10.1063/1.3467499, 2010.
762 Huba, J. D., and Rudakov, L. I.: Three-dimensional Hall magnetic reconnection, Phys.
763 Plasmas, 9, 4435, 2002.
764 Hudson, P. D., Discontinuities in an anisotropic plasma and their identification in the solar
765 wind, Planet. Space Sci., 18, 1611–1622, 1970.
766 Jain, N., Büchner, J., Dorfman, S., Ji, H., and Sharma, A. S.: Current disruption and its spreading
767 in collisionless magnetic reconnection, Phys. Plasmas 20, 112101, 2013.
768 Komar, C. M., Cassak, P. A., Dorelli, J. C., Glocer, A., and Kuznetsova, M. M., Tracing magnetic
769 separators and their dependence on IMF clock angle in global magnetospheric simulations, J.
770 Geophys. Res. Space Physics, 118, 4998–5007, doi:10.1002/jgra.50479, 2013.
771 Kuo, H., Russell, C. T., and Le, G., Statistical studies of flux transfer events, *J. Geophys.*
772 *Res.*, 100(A3), 3513–3519, doi: 10.1029/94JA02498, 1995.
773 Laitinen, T. V., Janhunen, P., Pulkkinen, T. I., Palmroth, M., and Koskinen, H. E. J., On the
774 characterization of magnetic reconnection in global MHD simulations, *Ann.*
775 *Geophys.*, **24**, 3059–3069, 2006.
776 Laitinen, T. V., Palmroth, M., Pulkkinen, T. I., Janhunen, P., and Koskinen, H. E. J.: Continuous
777 reconnection line and pressure-dependent energy conversion on the magnetopause in a global
778 MHD model, *J. Geophys. Res.*, **112**, A11201, doi:10.1029/2007JA012352, 2007.
779 Lapenta, G., Krauss-Varban, D., Karimabadi, H., Huba, J. D., Rudakov, L. I., and Ricci,
780 P.: Kinetic simulations of X-line expansion in 3D reconnection, Geophys. Res. Lett., 33,
781 L10102, doi:10.1029/2005GL025124, 2006.
782 Lee, L. C., and Fu, Z. F., A theory of magnetic flux transfer at the earth's

783 magnetopause, *Geophys. Res. Lett.*, **12**, 105, 1985.
784 Lockwood, M., Sandholt, P. E., and Cowley, S. W. H.: Dayside auroral activity and momentum
785 transfer from the solar wind, *Geophys. Res. Lett.*, **16**, 33, 1989.
786 Lockwood, M., and Smith, M. F.: Low altitude signatures of the cusp and flux transfer
787 events, *Geophys. Res. Lett.*, **16**, 879–882, 1989.
788 Lockwood, M., Cowley, S. W. H., Sandholt, P. E., and Lepping, R. P., The ionospheric
789 signatures of flux transfer events and solar wind dynamic pressure changes, J. Geophys.
790 Res., 95(A10), 17113–17135, doi:10.1029/JA095iA10p17113, 1990.
791 Lockwood, M., and Smith, M. F., Low and middle altitude cusp particle signatures for general
792 magnetopause reconnection rate variations: 1. Theory, *J. Geophys. Res.*, 99(A5), 8531–
793 8553, doi:10.1029/93JA03399, 1994.
794 Lockwood, M., et al: Co-ordinated Cluster and ground-based instrument observations of
795 transient changes in the magnetopause boundary layer during an interval of predominantly
796 northward IMF: Relation to reconnection pulses and FTE signatures, *Ann.*
797 *Geophys.*, **19**, 1613–1640, doi:10.5194/angeo-19-1613-2001, 2001.
798 Luhmann, J. G., Walker, R. J., Russell, C. T., Crooker, N. U., Spreiter, J. R., and Stahara, S. S.:
799 Patterns of potential magnetic field merging sites on the dayside magnetopause, *J. Geophys.*
800 *Res.*, **89**, 1739–1742, doi:10.1029/JA089iA03p01739, 1984.
801 Lui, A. T. Y., and Sibeck, D. G.: Dayside auroral activities and their implications for impulsive
802 entry processes in the dayside magnetosphere, *J. Atmos. Terr. Phys.*, **53**, 219, 1991.
803 McFadden, J. P., et al., The THEMIS ESA plasma instrument and in-flight calibration, *Space Sci.*
804 *Rev.*, **141**, 277–302, 2008.
805 McWilliams, K. A., Yeoman, T. K., and Provan, G.: A statistical survey of dayside pulsed

ionospheric flows as seen by the CUTLASS Finland HF radar, Ann. Geophys., 18, 445–453, doi:10.1007/s00585 - 000 - 0445 - 8, 2000.

McWilliams, K. A., Yeoman, T.K., and Cowley, S.W.H.: Two-dimensional electric field measurements in the ionospheric footprint of a flux transfer event, Annales Geophysicae, 18, pp. 1584–1598, 2001a.

McWilliams, K. A., Yeoman, T.K., Sigwarth, J.B., Frank, L.A., and Brittnacher, M.:The dayside ultraviolet aurora and convection responses to a southward turning of the interplanetary magnetic field, Annales Geophysicae, 17, pp. 707–721, 2001b.

McWilliams, K. A., Yeoman, T.K., Sibeck, D.G., Milan, S.E., Sofko, G.J., Nagai, T., Mukai, T., Coleman, I.J., Hori, T., and Rich, F.J., Simultaneous observations of magnetopause flux transfer events and of their associated signatures at ionospheric altitudes, Annales Geophysicae, 22, pp. 2181–2199, 2004.

Milan, S. E., M. Lester, S. W. H. Cowley, and M. Brittnacher (2000), Convection and auroral response to a southward turning of the IMF: Polar UVI, CUTLASS, and IMAGE signatures of transient magnetic flux transfer at the magnetopause, J. Geophys. Res., 105(A7), 15741–15755, doi:10.1029/2000JA900022.

Milan, S. E., Imber, S. M., Carter, J. A., Walach, M.-T., and Hubert, B.: What controls the local time extent of flux transfer events?, J. Geophys. Res. Space Physics, 121, 1391–1401, doi:10.1002/2015JA022012, 2016.

Moen, J., Carlson, H. C., Milan, S. E., Shumilov, N., Lybekk, B., Sandholt, P. E., and Lester, M.: On the collocation between dayside auroral activity and coherent HF radar backscatter, Ann. Geophys., 18, 1531-1549, https://doi.org/10.1007/s00585-001-1531-2, 2000.

Nakamura, T. K. M., Nakamura, R., Alexandrova, A., Kubota, Y., and Nagai, T.: Hall

magnetohydrodynamic effects for three-dimensional magnetic reconnection with finite width along the direction of the current, J. Geophys. Res., 117, A03220, doi:10.1029/2011JA017006, 2012.

Neudegg, D. A., Yeoman, T. K., Cowley, S. W. H., Provan, G., Haerendel, G., Baumjohann, W., Auster, U., Fornacon, K.-H., Georgescu, E., and Owen, C. J.: A flux transfer event observed at the magnetopause by the Equator-S spacecraft and in the ionosphere by the CUTLASS HF radar, Ann. Geophysicae, 17, 707, 1999.

Neudegg, D. A., et al., A survey of magnetopause FTEs and associated flow bursts in the polar ionosphere, *Ann. Geophys.*, **18**, 416, 2000.

Nishitani, N., Ogawa, T., Pinnock, M., Freeman, M. P., Dudeney, J. R., Villain, J.-P., Baker, K. B., Sato, N., Yamagishi, H., and Matsumoto, H.: A very large scale flow burst observed by the SuperDARN radars, J. Geophys. Res., 104(A10), 22469–22486, doi:10.1029/1999JA900241, 1999.

Newell, P. T., Meng, C.-I., Sibeck, D. G., and Lepping, R.: Some low-altitude cusp dependencies on the interplanetary magnetic field, J. Geophys. Res., 94(A7), 8921–8927, doi:10.1029/JA094iA07p08921, 1989.

Newell P. T., and Meng C.-I.: Ion acceleration at the equatorward edge of the cusp: Low-altitude observations of patchy merging, Geophys. Res. Lett., 18, 1829–1832, doi:10.1029/91GL02088, 1991.

Newell, P. T., and Meng, C. - I : Ionospheric projections of magnetospheric regions under low and high solar wind conditions, J. Geophys. Res., 99, 273, 1994.

Newell, P. T., Sotirelis, T., Liou, K., Meng, C. - I. and Rich, F. J., A nearly universal solar wind - magnetosphere coupling function inferred from 10 magnetospheric state variables, J.

852 Geophys. Res., 112, A01206, doi: 10.1029/2006JA012015, 2007b.
853 Tsyganenko, N. A., Modeling the Earth's magnetospheric magnetic field confined within a
854 realistic magnetopause, J. Geophys. Res., 100(A4), 5599–5612, doi:10.1029/94JA03193,
855 1995.
856 Oksavik, K., Moen, J. and Carlson, H. C.: High-resolution observations of the small-scale flow
857 pattern associated with a poleward moving auroral form in the cusp, *Geophys. Res.*
858 *Lett.*, **31**, L11807, doi:10.1029/2004GL019838, 2004.
859 Oksavik, K., Moen, J., Carlson, H. C., Greenwald, R. A., Milan, S. E., Lester, M., Denig, W. F.,
860 and Barnes, R. J.: Multi-instrument mapping of the small-scale flow dynamics related to a
861 cusp auroral transient, *Ann. Geophys.*, **23**, 2657–2670, 2005.
862 Paschmann, G., et al.: Plasma acceleration at the Earth's magnetopause: Evidence for magnetic
863 reconnection, Nature, 282, 243, 1979.
864 Paschmann, G., et al.: The magnetopause for large magnetic shear: AMPTE/IRM
865 observations, *J. Geophys. Res.*, **91**, 11,099, 1986.
866 Petrinec, S. M., and Fuselier, S. A.: On continuous versus discontinuous neutral lines at the
867 dayside magnetopause for southward interplanetary magnetic field, Geophys. Res.
868 Lett., 30(10), 1519, doi:10.1029/2002GL016565, 2003.
869 Phan, T. D., and Paschmann, G.: Low‐latitude dayside magnetopause and boundary layer for
870 high magnetic shear: 1. Structure and motion, J. Geophys. Res., 101, 7801–7815,
871 doi:10.1029/95JA03752, 1996.
872 Phan, T.-D., et al.: Extended magnetic reconnection at the Earth's magnetopause from detection
873 of bi-directional jets, *Nature*, **404**, 848, 2000.
874 Phan, T.D., Freeman, M.P., Kistler, L.M. et al, Evidence for an extended reconnection line at the

dayside magnetopause, Earth Planet Sp 53: 619. https://doi.org/10.1186/BF03353281, 2000.

Phan, T., et al.: Simultaneous Cluster and IMAGE observations of cusp reconnection and auroral proton spot for northward IMF, Geophys. Res. Lett., 30(10), 1509, doi:10.1029/2003GL016885, 2003.

Phan, T. D., Hasegawa, H., Fujimoto, M., Oieroset, M., Mukai, T., Lin, R. P., and Paterson, W. R.: Simultaneous Geotail and Wind observations of reconnection at the subsolar and tail flank magnetopause, Geophys. Res. Lett., 33, L09104,doi:10.1029/2006GL025756, 2006.

Phan, T. D., Paschmann, G., Gosling, J. T., Oieroset, M., Fujimoto, M., Drake, J. F., and Angelopoulos, V.: The dependence of magnetic reconnection on plasma β and magnetic shear: Evidence from magnetopause observations, Geophys. Res. Lett., 40, 11–16, doi:10.1029/2012GL054528, 2013.

Pinnock, M., Rodger, A. S., Dudeney, J. R., Baker, K. B., Newell, P. T., Greenwald, R. A., and Greenspan, M. E.: Observations of an enhanced convection channel in the cusp ionosphere, J. Geophys. Res., 98, 3767–3776, 1993.

Pinnock, M., Rodger, A. S., Dudeney, J. R., Rich, F., and Baker, K. B.: High spatial and temporal resolution observations of the ionospheric cusps, *Ann. Geophys.*, **13**, 919–925, 1995.

Pinnock, M & Rodger, A., On determining the noon polar cap boundary from SuperDARN HF radar backscatter characteristics. Annales Geophysicae. 18. 10.1007/s00585-001-1523-2, 2001.

Pinnock, M., Chisham, G., Coleman, I. J., Freeman, M. P., Hairston, M., and Villain, J.-P.: The location and rate of dayside reconnection during an interval of southward interplanetary magnetic field, Ann. Geophys., 21, 1467–1482, 2003.

898 Plaschke F, Hietala H., Angelopoulos V.: Anti-sunward high-speed jets in the subsolar
899 magnetosheath. Ann. Geophys. 2013;31:1877–1889. doi:10.5194/angeo-31-1877-2013,
900 2013.
901 Ponomarenko, P. V., Waters, C. L., and Menk, F. W.: Factors determining spectral width of HF
902 echoes from high latitudes, Ann. Geophys., 25, 675-687, https://doi.org/10.5194/angeo-25-
903 675-2007, 2007.
904 Provan, G. & Yeoman, T.K.: Statistical observations of the MLT, latitude and size of pulsed
905 ionospheric flows with the CUTLASS Finland radar, Annales Geophysicae, 17: 855.
906 https://doi.org/10.1007/s00585-999-0855-1, 1999.
907 Provan, G., Yeoman, T. K., and Milan, S. E., CUTLASS Finland radar observations of the
908 ionospheric signatures of flux transfer events and the resulting plasma flows, *Ann.*
909 *Geophys.*, **16**, 1411–1422, 1998.
910 Ruohoniemi, J. M., Greenwald, R. A., Baker, K. B., Villain, J.-P., Hanuise, C., and Kelly,
911 J.: Mapping high-latitude plasma convection with coherent HF radars, J. Geophys.
912 Res., 94(A10), 13463–13477, doi:10.1029/JA094iA10p13463, 1989.
913 Ruohoniemi, J. M., and Baker, K. B.: Large-scale imaging of high-latitude convection with
914 Super Dual Auroral Radar Network HF radar observations, J. Geophys.
915 Res., 103(A9), 20797–20811, doi:10.1029/98JA01288, 1998.
916 Russell, C. T., and Elphic, R. C.: ISEE observations of flux transfer events at the dayside
917 magnetopause, Geophys. Res. Lett., 6(1), 33–36, doi:10.1029/GL006i001p00033, 1979.
918 Sandholt, P. E., Deehr, C. S., Egeland, A., Lybekk, B., Viereck, R., and Romick, G.
919 J.: Signatures in the dayside aurora of plasma transfer from the magnetosheath, J. Geophys.
920 Res., 91(A9), 10063–10079, doi:10.1029/JA091iA09p10063, 1986.

921 Sandholt, P. E., Lockwood, M., Oguti, T., Cowley, S. W. H., Freeman, K. S. C., Lybekk, B.,
922 Egeland, A., and Willis, D. M.: Midday auroral breakup events and related energy and
923 momentum transfer from the magnetosheath, J. Geophys. Res., 95(A2), 1039–1060,
924 doi:10.1029/JA095iA02p01039, 1990.
925 Sandholt, P. E., et al.: Cusp/cleft auroral activity in relation to solar wind dynamic pressure,
926 interplanetary magnetic field B_z and B_y , J. Geophys. Res., 99(A9), 17323–17342,
927 doi:10.1029/94JA00679, 1994.
928 Scholer, M.: Magnetic flux transfer at the magnetopause based on single x line bursty
929 reconnection, *Geophys. Res. Lett.*, **15**, 291, 1988.
930 Scholer, M., Sidorenko, I., Jaroschek, C. H., Treumann, R. A., and Zeiler, A.: Onset of
931 collisionless magnetic reconnection in thin current sheets: Three-dimensional particle
932 simulations, *Phys. Plasmas*, **10**(9), 3521–3527, 2003.
933 Shay, M. A., Drake, J. F., Swisdak, M., Dorland, W., and Rogers, B. N.: Inherently three
934 dimensional magnetic reconnection: A mechanism for bursty bulk flows? Geophys. Res.
935 Lett., 30(6), 1345, doi:10.1029/2002GL016267, 2003.
936 Shepherd, L. S., and Cassak, P. A.: Guide field dependence of 3-D X-line spreading during
937 collisionless magnetic reconnection, J. Geophys. Res., 117, A10101,
938 doi:10.1029/2012JA017867, 2012.
939 Smith, M., Lockwood, F.M., Cowley, S.W.H.: The statistical cusp: a simple flux transfer event
940 model, *Planet Space Sci.*, 1992
941 Sonnerup, B. U. Ö., and Cahill Jr., L. J.: Magnetopause structure and attitude from Explorer 12
942 observations, *J. Geophys. Res.*, **72**, 171, 1967.
943 Sonnerup, B. U.: Magnetopause reconnection rate, J. Geophys. Res., 79(10), 1546–1549,

doi:10.1029/JA079i010p01546, 1974.

Southwood, D. J.: Theoretical aspects of ionosphere - magnetosphere - solar wind coupling, Adv. Space Res., 5(4), 7–14, doi:10.1016/0273 - 1177(85)90110 - 3, 1985.

Southwood, D. J.: The ionospheric signature of flux transfer events, *J. Geophys. Res.*, **92**, 3207, 1987.

Southwood, D. J., Farrugia, C. J., and Saunders, M. A.: What are flux transfer events? *Planet. Space Sci.*, **36**, 503, 1988.

Thorolfsson, A., Cerisier, J.-C., Lockwood, M., Sandholt, P. E., Senior, C. and Lester, M.: Simultaneous optical and radar signatures of poleward-moving auroral forms, *Ann. Geophys.*, **18**, 1054, 2000.

Trattner, K. J., Fuselier, S. A., and Petrinec, S. M.: Location of the reconnection line for northward interplanetary magnetic field, J. Geophys. Res., 109, A03219, doi:10.1029/2003JA009975, 2004.

Trattner, K. J., Mulcock, J. S., Petrinec, S. M., and Fuselier, S. A.: Probing the boundary between antiparallel and component reconnection during southward interplanetary magnetic field conditions, *J. Geophys. Res.*, 112, A08210, doi:10.1029/2007JA012270, 2007.

Trattner, K. J., Fuselier, S. A., Petrinec, S. M., Yeoman, T. K., Escoubet, C. P., and Reme, H.: The reconnection sites of temporal cusp structures, J. Geophys. Res., 113, A07S14, doi:10.1029/2007JA012776, 2008.

Trattner, K. J., Burch, J. L., Ergun, R., Eriksson, S., Fuselier, S. A., Giles, B. L., … Wilder, F. D. :The MMS dayside magnetic reconnection locations during phase 1 and their relation to the predictions of the maximum magnetic shear model. Journal of Geophysical Research: Space Physics, 122, 11,991–12,005. https://doi.org/10.1002/2017JA024488, 2017.

967 Trenchi, L., Marcucci, M. F., Pallocchia, G., Consolini, G., Bavassano Cattaneo, M. B., Di
968 Lellis, A. M., Rème, H., Kistler, L., Carr, C. M., and Cao, J. B.: Occurrence of reconnection
969 jets at the dayside magnetopause: Double star observations, J. Geophys. Res., 113, A07S10,
970 doi:10.1029/2007JA012774, 2008.
971 Tsyganenko, N. A.: A magnetospheric magnetic field model with a warped tail current sheet,
972 Planet. Space Sci., 87, 5, 1989
973 Tsyganenko, N. A.: Modeling the Earth's magnetospheric magnetic field confined within a
974 realistic magnetopause, J. Geophys. Res., 100(A4), 5599–5612, doi:10.1029/94JA03193,
975 1995.
976 Tsyganenko, N. A.: A model of the magnetosphere with a dawn-dusk asymmetry, 1,
977 Mathematical structure, J. Geophys. Res., 107(A8), doi:10.1029/2001JA000219, 2002a.
978 Tsyganenko, N. A.: A model of the near magnetosphere with a dawn-dusk asymmetry, 2,
979 Parameterization and fitting to observations, J. Geophys. Res., 107(A8),
980 doi:10.1029/2001JA000220, 2002b.
981 Walsh, B. M., Foster, J. C., Erickson, P. J., and Sibeck, D. G.: Simultaneous ground- and space-
982 based observations of the plasmaspheric plume and reconnection, *Science*, **343**, 1122–1125,
983 doi:10.1126/science.1247212, 2014a.
984 Walsh, B. M., Phan, T. D., Sibeck, D. G., and Souza, V. M.: The plasmaspheric plume and
985 magnetopause reconnection, Geophys. Res. Lett., 41, 223–228, doi:10.1002/2013GL058802,
986 2014b.
987 Walsh, B. M., Komar, C. M., and Pfau-Kempf, Y.: Spacecraft measurements constraining the
988 spatial extent of a magnetopause reconnection X line, Geophys. Res. Lett., 44, 3038–3046,
989 doi:10.1002/2017GL073379, 2017.

990 Wang, Y., et al.: Initial results of high-latitude magnetopause and low-latitude flank flux transfer
991 events from 3 years of Cluster observations, J. Geophys. Res., 110, A11221,
992 doi:10.1029/2005JA011150, 2005.
993 Wang, J., et al., TC1 and Cluster observation of an FTE on 4 January 2005: A close
994 conjunction, Geophys. Res. Lett., 34, L03106, doi:10.1029/2006GL028241, 2007.
995 Wild, J. A., Cowley, S. W. H., Davies, J. A., Khan, H., Lester, M., Milan, S. E., Provan, G.,
996 Yeoman, T. K., Balogh, A., Dunlop, M. W., Fornacon, K.-H., and Georgescu, E.: First
997 simultaneous observations of flux transfer events at the high-latitude magnetopause by the
998 Cluster spacecraft and pulsed radar signatures in the conjugate ionosphere by the CUTLASS
999 and EISCAT radars, Ann. Geophys., 19, 1491–1508, 2001.
1000 Wild, J. A., Milan, S. E., Davies, J. A., Cowley, S. W. H., Carr, C. M., and Balogh, A.: Double
1001 Star, Cluster, and groundbased observations of magnetic reconnection during an interval of
1002 duskward oriented IMF: preliminary results, Ann. Geophys., 23, 2903–2907, 2005.
1003 Wild, J. A., Milan, S. E., Davies, J. A., Dunlop, M. W., Wright, D. M., Carr, C. M., Balogh, A.,
1004 Reme, H., Fazakerley, A. N., ` and Marchaudon, A.: On the location of dayside magnetic
1005 reconnection during an interval of duskward oriented IMF, Ann. Geophys., 25, 219–238,
1006 2007.
1007 Zhang, Q.-H., et al.: Simultaneous tracking of reconnected flux tubes: Cluster and conjugate
1008 SuperDARN observations on 1 April 2004, *Ann. Geophys.*, **26**, 1545–1557,
1009 doi:10.5194/angeo-26-1545-2008, 2008.
1010 Zou, Y., Walsh, B. M., Nishimura, Y., Angelopoulos, V., Ruohoniemi, J. M., McWilliams, K.
1011 A., & Nishitani, N. Spreading speed of magnetopause reconnection X-lines using ground-
1012 satellite coordination. Geophysical Research Letters, 45.

https://doi.org/10.1002/2017GL075765, 2018.

Figure 1a: OMNI IMF condition on Feb 2, 2013. Figure 1b: THE and THA locations projected to the GSM X-Y plane. The inner curve marks the magnetopause and the outer curve marks the bow shock.

Figure 2a: SuperDARN LOS speeds (color tiles) and merged velocity vectors (color arrows) in the Altitude adjusted corrected geomagnetic (*AACGM*) coordinates. The FOVs of the RKN, INV, and CLY radars are outlined with the black dashed lines. The colors of the tiles indicate the LOS speeds away from the radar. The colors and the lengths of the arrows indicate the merged velocity magnitudes and the arrow directions indicate the velocity directions. Red and anti-sunward directed flows are the ionospheric signature of magnetopause reconnection. The dashed magenta lines mark the flow western and eastern boundaries. The open-closed field line boundary was delineated by the dashed black curve marked by the "OCB" marker. The satellite footprints under the T89 are shown as the THE and THA marker. Figure 2b: Similar to Figure 2a but showing SECS velocity vectors (color arrows). Figure 2c: Similar to Figure 2a but showing SHF velocity vectors (color arrows). Figure 2d: SuperDARN spectral width measurements (color tiles). The red contour marks localized enhanced soft electron precipitation. Figure 2e: Time evolution of the northward component of SECS velocities along 79° MLAT. Figure 2f: Profile of convection velocities along 79° MLAT at 1929 UT as a function of the distance from magnetic noon. The profile in black is based on the LOS measurements and the profile in red is the northward component of the SECS velocities. The FWHM is determined based on each profile. Figures 2g-j: THE measured magnetic field (0.25 s resolution), ion energy flux (3 s), ion density (3 s), and ion velocity (3 s). The ion measurements were taken from ground ESA moments. The magnetic field and the ion velocity components are displayed in the LMN boundary normal coordinate system.

The magnetopause crossing is shaded in pink. Figure 2k: THE ion distribution function on the bulk velocity-magnetic field plane. The small black line indicates the direction and the bulk velocity of the distributions. Figures 2l-p: THA measurements in the same format as in Figures 2g-k. Figures 2q-z: THA and THE measurements during a subsequent magnetopause crossing shown in the same format as in Figures 2g-p.

Figures 3a-c: Snapshots of spectral width measurements around the space-ground conjunction time and longitude. The open-closed field line boundary is drawn as the dashed black line. Figures 3d-f: time series of the spectral width measurements along INV beams 4, 7, and 10, as a function of latitude, from which the motion of the open-closed field line boundary can be derived. Figure 3g: the electric field along the open-closed field line boundary in the frame of boundary (solid) and in the rest frame (dashed) following Pinnock et al. [2003], Freeman et al. [2007], Chisham et al. [2008]. The former is the reconnection electric field.

Figure 4: OMNI IMF condition and THEMIS satellite locations on Apr 19, 2015 in a similar format to Figure 1.

Figure 5. THEMIS and SuperDARN measurements of reconnection bursts on Apr 19, 2015 in a similar format to Figure 2. The velocity time evolution in Figure 5e and the velocity profile in Figure 5f are taken along 78° MLAT.

Figure 6. OMNI IMF condition and THEMIS satellite locations on Apr 29, 2015 in a similar format to Figure 1.

Figure 7. THEMIS and SuperDARN measurements of reconnection bursts on Apr 29, 2015 in a similar format to Figure 2. The velocity time evolution in Figure 7e and the velocity profile in Figure 7f are taken along 79° MLAT. The two branches of the LOS velocity profile in Figure 7f are based on INV and RKN LOS data. The magnetic field and plasma velocities measured by spacecraft are displayed in the GSM coordinates.

Figure 8. Comparison of the IMF and solar wind driving conditions between the reconnection events on Feb 2, 2013, Apr 19, 2015, and Apr 29, 2015. From top to bottom: IMF in GSM coordinates, IMF clock angle, solar wind speed, and solar wind dynamic pressure. The red vertical lines mark the times of the satellite-ground conjunction.

1096 Figure 1.

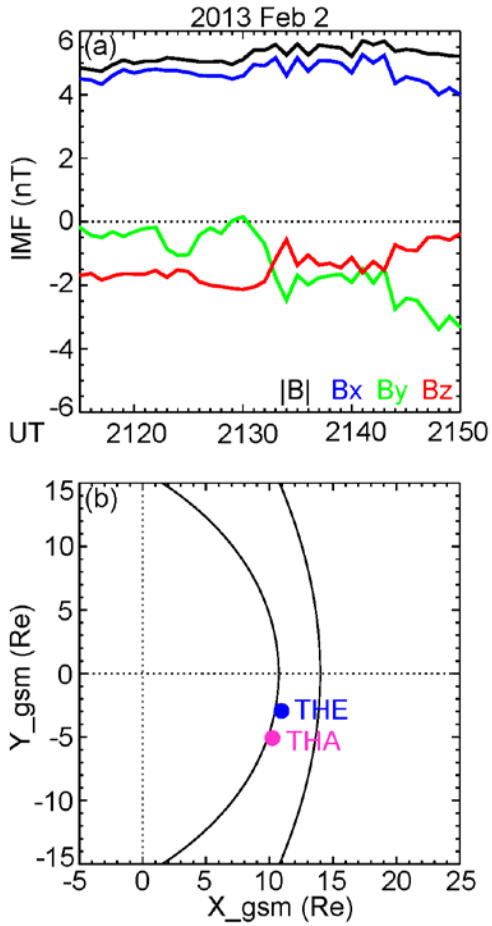

1097

1098

1099

1100

1101

1102

1103

1104 Figure 2.

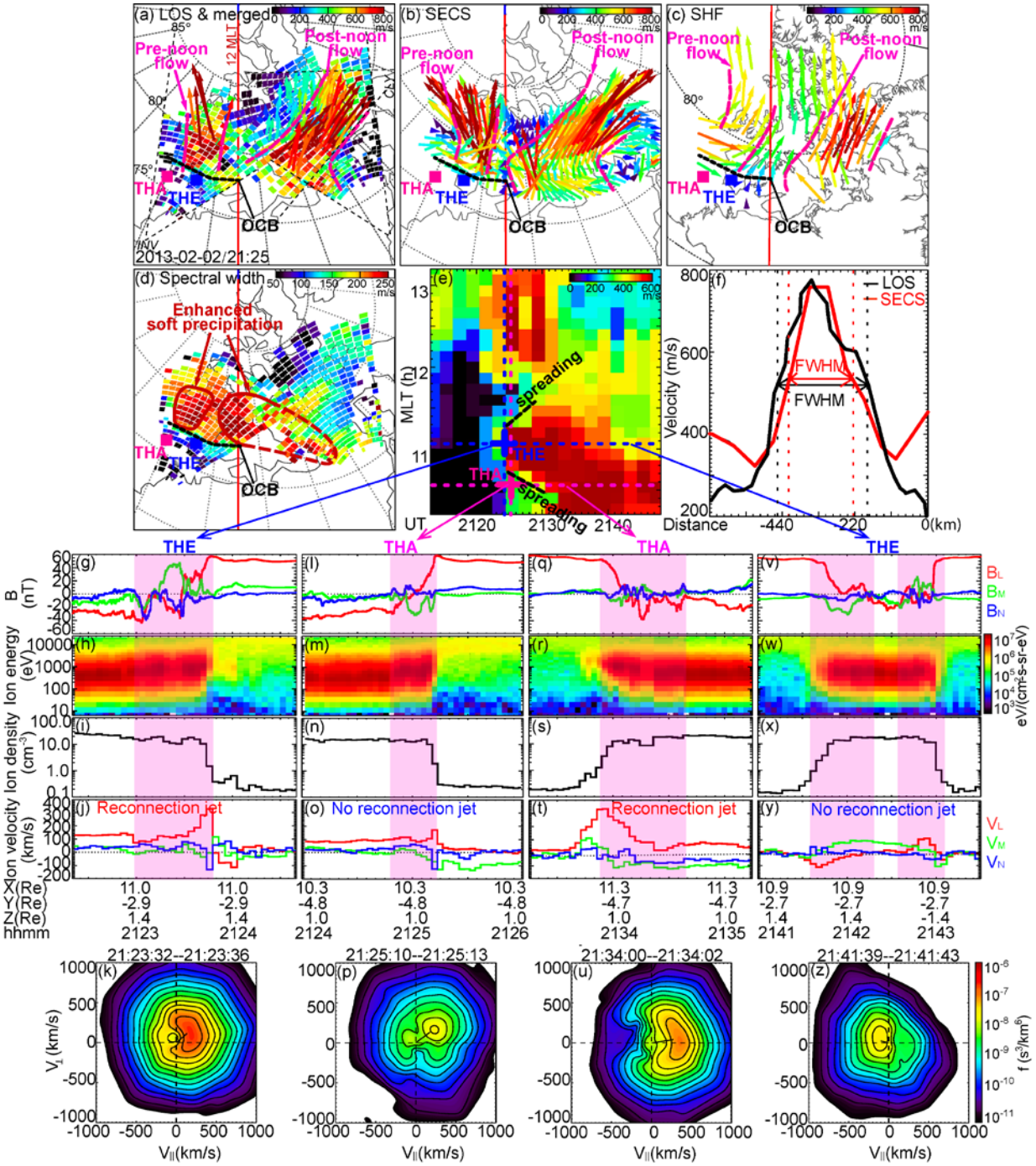

1105

1106

1107

1108

Figure 3.

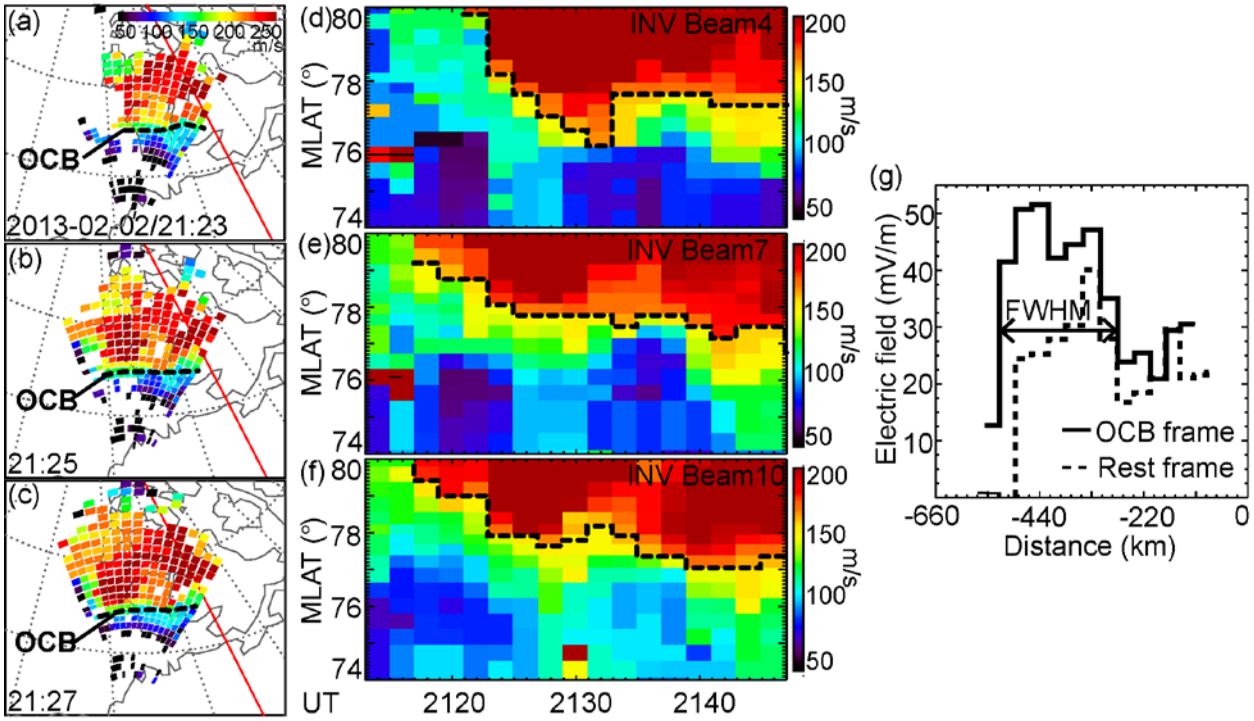
(a)
50 100 150 200 250
m/s
OCB
2013-02-02/21:23
(b)
OCB
21:25
(c)
OCB
21:27
(d)
INV Beam4
(e)
INV Beam7
(f)
INV Beam10
MLAT (°)
80
78
76
74
200
150
100
50
m/s
UT
2120
2130
2140
(g)
Electric field (mV/m)
50
40
30
20
10
FWHM
OCB frame
Rest frame
-660
-440
-220
0
Distance (km)

Figure 4.

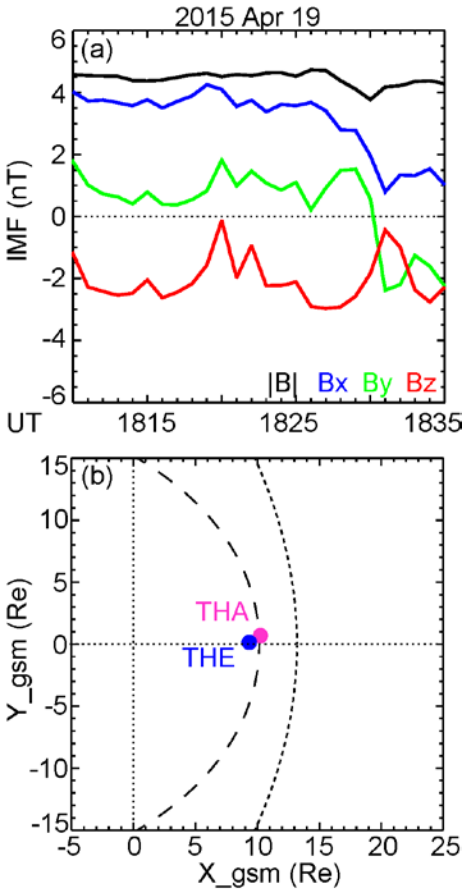
2015 Apr 19
(a)
IMF (nT)
|B| Bx By Bz
UT
1815
1825
1835
(b)
THA
THE
Y_gsm (Re)
X_gsm (Re)

1134 Figure 5.

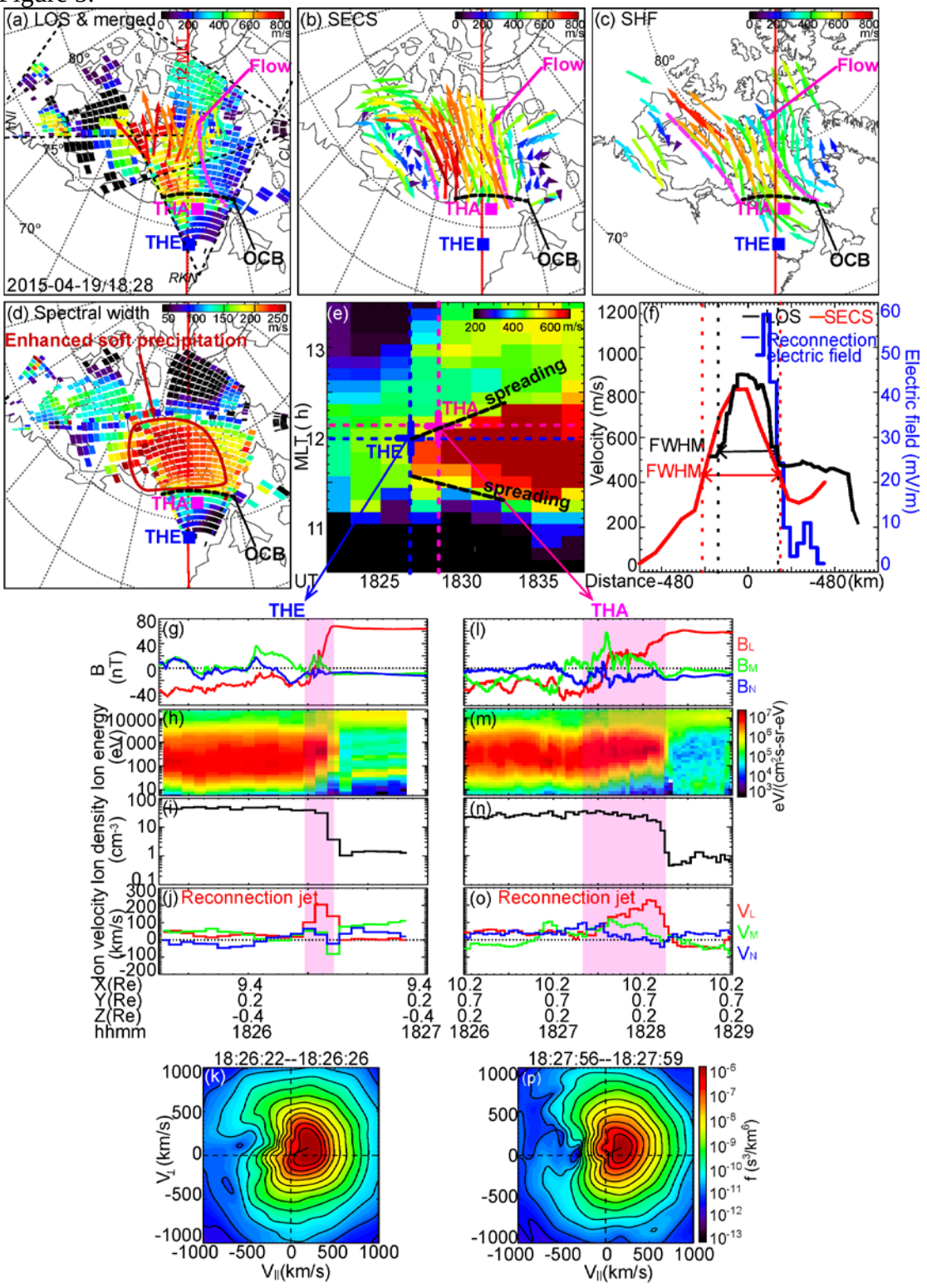

1135

Figure 6.

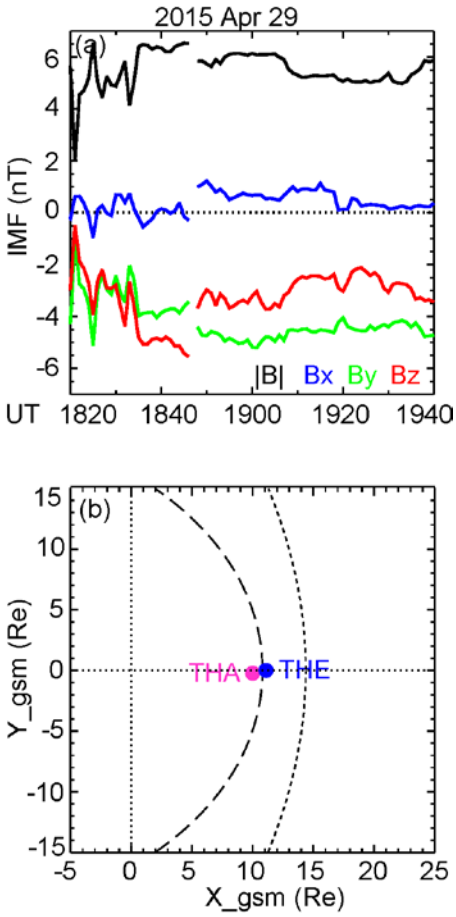
2015 Apr 29
(a)
IMF (nT)
|B| Bx By Bz
UT 1820 1840 1900 1920 1940
(b)
Y_gsm (Re)
X_gsm (Re)
THA
THE

1147 Figure 7.

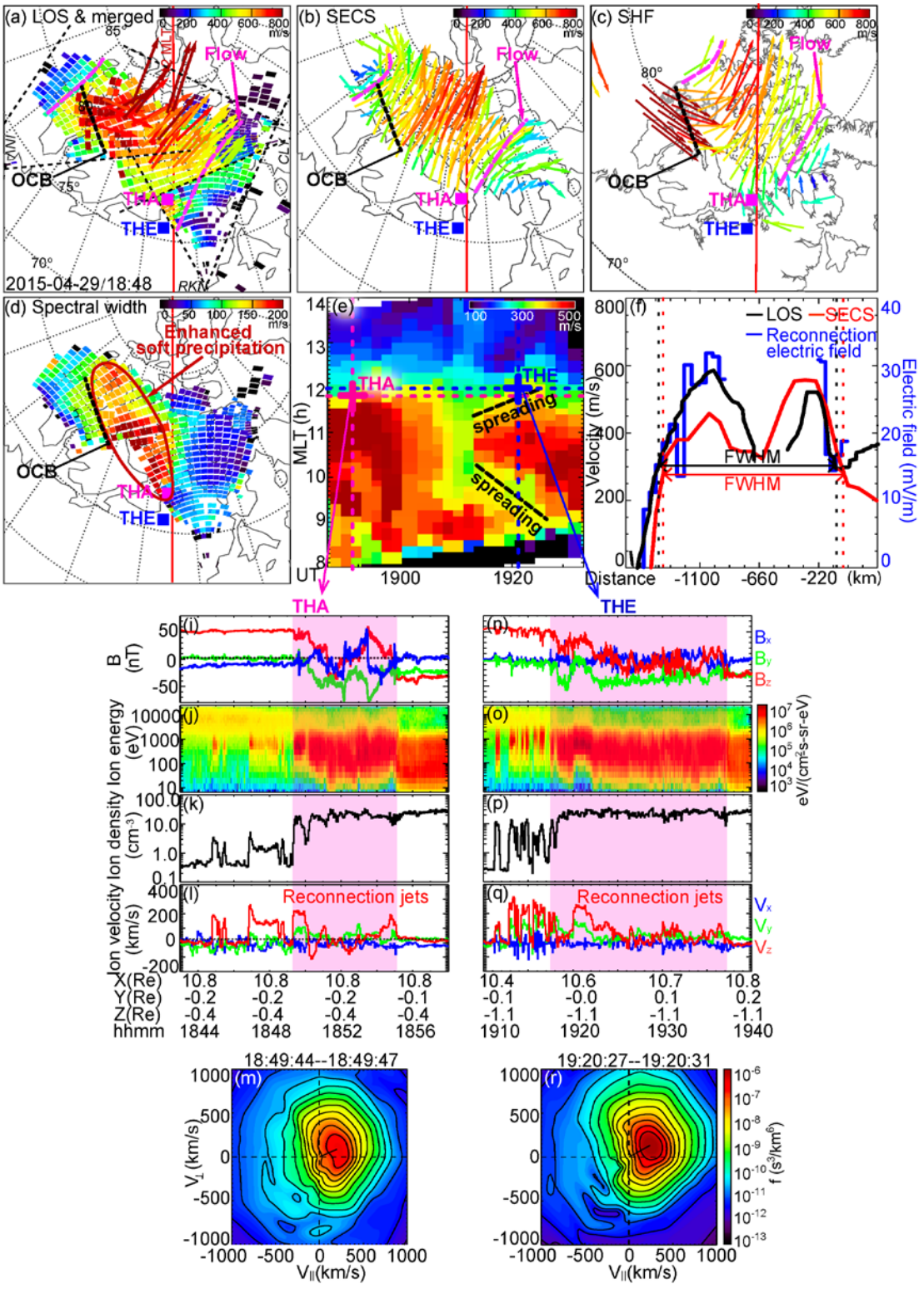

1148

1149

Figure 8.

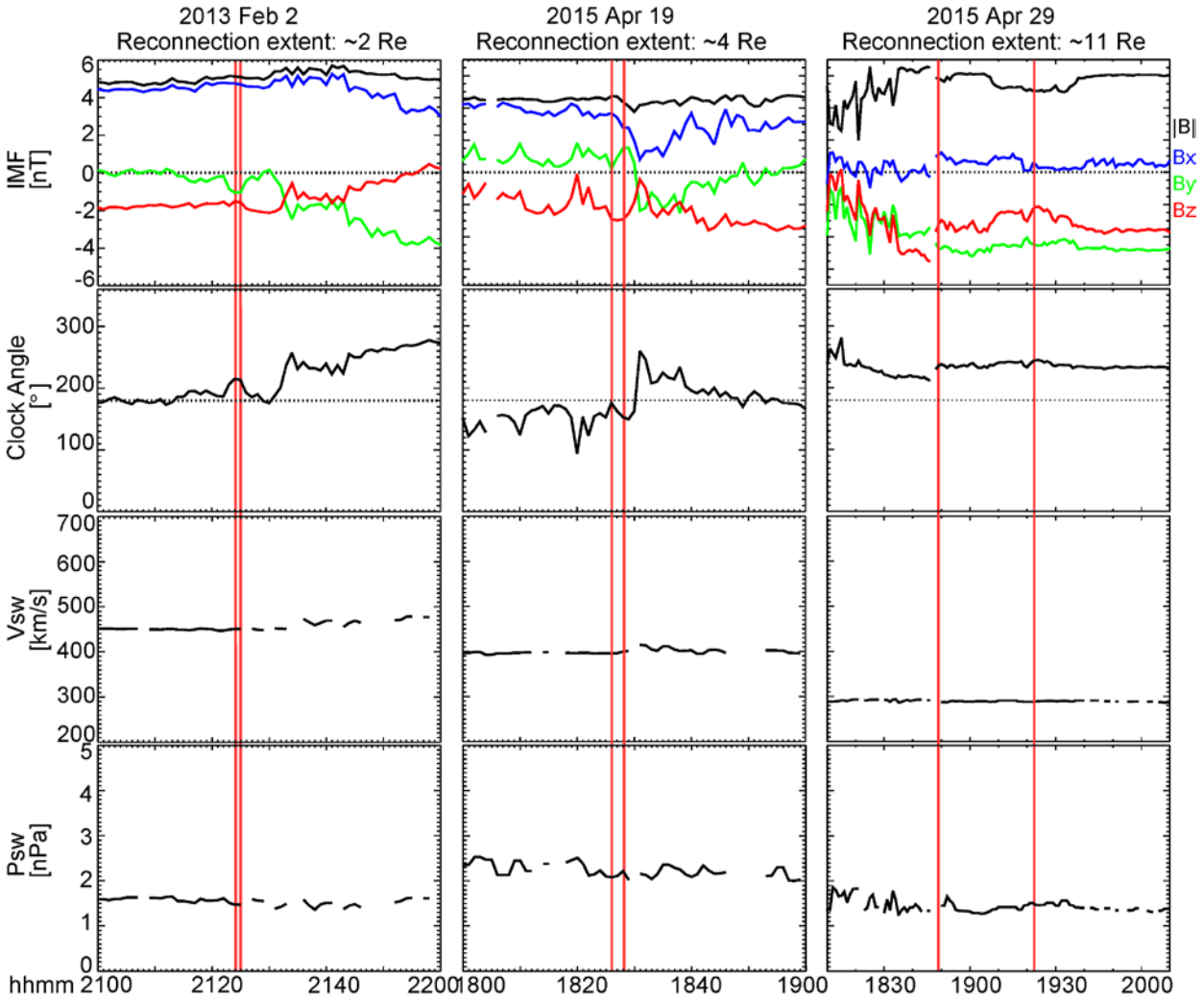
2013 Feb 2
Reconnection extent: ~2 Re
2015 Apr 19
Reconnection extent: ~4 Re
2015 Apr 29
Reconnection extent: ~11 Re
IMF [nT]
|B|
Bx
By
Bz
Clock Angle [°]
Vsw [km/s]
Psw [nPa]
hhmm
2100
2120
2140
2200
1800
1820
1840
1900
1830
1900
1930
2000